

UCSF

UC San Francisco Electronic Theses and Dissertations

Title

ApoE-Genotype-Specific Drug Repositioning Identifies Bumetanide as an Effective Compound in a Mouse Model of Alzheimer's Disease

Permalink

<https://escholarship.org/uc/item/7n9604sm>

Author

Taubes, Alice Lorraine

Publication Date

2019

Peer reviewed|Thesis/dissertation

ApoE-Genotype-Specific Drug Repositioning Identifies Bumetanide as an Effective Compound in a Mouse Model of Alzheimer's Disease

by
Alice Taubes

DISSERTATION

Submitted in partial satisfaction of the requirements for degree of
DOCTOR OF PHILOSOPHY

in

Biomedical Sciences

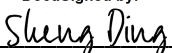
in the

GRADUATE DIVISION

of the

UNIVERSITY OF CALIFORNIA, SAN FRANCISCO

Approved:

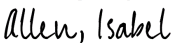
DocuSigned by:

8CDD680BE3E24BD... Sheng Ding
Chair

DocuSigned by:

Yadong Huang

DocuSigned by:

Marina Sirota

DocuSigned by:

3EB794DA2CB6405... Allen, Isabel

Committee Members

DEDICATION

This work is dedicated to my grandmother *Alice Sizer Warner*

ACKNOWLEDGEMENTS

I would like to acknowledge my mentor Dr. Yadong Huang, without whom this work would not be possible. Dr. Huang believed in my ability as a scientist before I did, has encouraged me every step of the way towards becoming the best scientist I can be, and continues to encourage me to achieve my dreams. He has given me confidence in myself as a scientist and as an individual, and I am incredibly grateful that I am lucky enough to have him as my mentor.

I would like to acknowledge my co-mentor Dr. Marina Sirota. Dr. Sirota accepted me as a student on blind faith that I could learn to code. She mentored me through learning how to be a successful computational scientist, and supported me at every stage of my project and beyond into my next steps. Without Dr. Sirota, I would never have been introduced to computational biology. I am incredibly lucky to have her support and mentorship.

I would further like to acknowledge my thesis committee members Dr. Sheng Ding and Dr. Isabel Allen. Dr. Ding provided invaluable guidance into drug repositioning techniques and helped to plan mechanistic experiments, and Dr. Allen was a fantastic resource for all of my questions regarding statistics, career steps, and the direction of this project.

This project would not have happened without the support, guidance, and time and input from all of the members of the Huang Lab. I have learned greatly from current and former lab members including Dr. Phil Nova, David Walker, Maureen (Reeny) Balestra, Dr. Qin Xu, Mary Jeong, Dr. Anna Gillespie, Dr. Leslie Tong, Dr. Johanna Knoeferle, Amy Wong, Dr. Chengzhong Wang, Victoria Yoon, Dr. Jessie Carr, Emily Jones, Ramsey Najm, Hung Lin, Dr. Kelly Zalocusky, Dr. Yanxia Hao, Dr. Min Xie, and Dr. Misha Zilberter. Dr. Phil Nova taught me how to dose mice and introduced me to the mechanisms by which Bumetanide works, David Walker taught me how to design and create cloning plasmids, Reeny Balestra supported me in

every way possible including teaching me cell culture and carried out cell culture experiments on my behalf. Emily Jones taught me how to code and helped me debug almost everything I wrote, and Dr. Anna Gillespie taught me how to dissect brains. Dr. Min Xie helped me with the chemistry of putting Bumetanide into solution. Ramsey Najm taught me cell culture and immunostaining and performed several cell-culture related experiments for this project on my behalf. Mary Jeong taught me how to do a western blot correctly. Dr. Kelly Zalocusky taught me how to be a better computational scientist and helped me think through and my computational pipelines. Victoria Yoon has worked tirelessly on so many aspects of this project on my behalf, was eternally patient and helpful on all aspects of this project, and is the reason this project is successful.

This project was also finished thanks to the invaluable support I received from several current and former members of the Sirota lab, including Dr. Silvia Pineda San Juan, Dr. Aolin Wang, Dr. Dmitry Rychkov, Dr. Leandro Lima, Dr. Idit Kosti, Dr. Hongtai Huang, Katherine Yu, and Brian Le and Manish Paranjpe. Dr. Silvia Pineda San Juan was incredibly generous with her time in helping me solve my statistics and R-related questions, Dr. Leandro Lima helped me solve coding questions I had, and Dr. Dmitry Rychkov was extremely helpful in his knowledge of R and coding.

I would like to acknowledge Dr. Bin Chen, who's code was instrumental in creating my computational pipeline, and who was extremely generous with his time to help me troubleshoot to create a streamlined pipeline. I would also like to acknowledge Dr. Boris Oskotsky, who helped me with all my server-related issues.

This work was supported by the J. David Gladstone Institute, the National Institutes of Health, and the Larry L. Hillblom Foundation.

CONTRIBUTIONS

Victoria (Seo Yeon) Yoon bred and maintained the all mouse lines used in this project, assisted in dosing mice for behavior, performed behavioral study lead-up (e.g. rodent transfers, single housing for behavior), and performed behavioral studies for the bumetanide-treated mice. Phil Nova provided additional assistance in dosing and behavioral testing. Dr. Misha Zilberter performed all electrophysiological experiments. Training for the behavior assays was provided by Dr. Michael Gill and Iris Lo of the Gladstone Behavior Core. Dr. Yanxia Hao and the Gladstone Genomics Core assisted in RNA extraction for the RNA-seq studies. Dr. Bin Chen provided drug repositioning pipeline code and data. Drs. Yadong Huang and Dr. Marina Sirota conceived of the original ideas for the studies presented here. Dr. Sirota conducted the background work on drug repositioning and Dr. Huang conducted the background work on ApoE and Alzheimer's disease.

ABSTRACT

Apolipoprotein E Genotype–Specific Drug Repositioning Identifies Bumetanide as an Effective Compound to Rescue Cognitive Deficits in a Mouse Model of Alzheimer’s Disease

By: Alice Taubes

Alzheimer’s disease (AD) is the leading cause of dementia worldwide, and no effective therapies are available. The multifactorial etiology and pathophysiological complexity of AD cause patient heterogeneity and pose challenges for drug development, with almost all efforts to target AD-related pathways having failed in human trials^{1,2}. Although apolipoprotein (apo) E4 is the major genetic risk factor for AD^{1,3-5}—60–80% of patients have at least one *APOE4* allele and ~70% of homozygotes develop AD by age 85^{6,7}—it has not been actively considered in drug target stratification and development for AD^{1,2}. Here, we used an apoE-genotype-specific drug repositioning approach to screen for drugs to treat apoE4-related AD. From a meta-analysis of 610 human temporal lobar samples from public databases, we established apoE-genotype-specific transcriptomic signatures of AD and applied them to a validated Connectivity Map (CMap) database containing transcriptomic perturbation signatures of 1300 existing drugs⁸ to identify those capable of perturbing an entire gene-expression network away from the apoE-genotype-driven disease state towards a normal state. The loop-diuretic bumetanide was the top predicted drug candidate for apoE4/4 AD. Treating aged apoE4 knock-in (apoE4-KI) mice with bumetanide rescued cognitive and neuronal plasticity deficits, warranting further efficacy tests in AD clinical trials. This study highlights the power of combining precision medicine, computational drug repositioning, and targeting network alterations in developing new therapies for AD and other neurodegenerative disorders.

TABLE OF CONTENTS

Chapter 1: Introduction	1
1.1 Alzheimer’s Disease and ApoE4.....	2
1.2 Disadvantages of Pathway-Based Drug Development Efforts.....	5
1.3 Precision Medicine, Disease Modelling, and Alzheimer’s Disease.....	5
1.4 Drug Repositioning and AD Drug Development.....	7
1.5 The Connectivity Map and Pharmacogenomics.....	8
1.6 Methods of Drug Repositioning.....	10
1.7 Bumetanide as a Repurposed Therapeutic Compound.....	11
1.8 Research Purpose.....	12
Chapter 2: Materials and Methods	13
2.1 Data Integration.....	14
2.2 Differential Expression and Pathway Analysis.....	15
2.3 Drug Repositioning Analysis.....	16
2.4 Mice.....	17
2.5 Bumetanide Treatment.....	18
2.6 Behavior Testing.....	18
2.7 RNA-Seq Analysis of Hippocampal Tissue.....	19
2.8 Brain Slice Electrophysiological Recordings and Data Analysis.....	21
2.9 Statistical Analysis.....	21
2.10 Compliance with Relevant Ethical Regulations and Animal Use Guidelines.....	21
Chapter 3: Bumetanide is Predicted to be Efficacious Against ApoE4-Mediated AD	22
3.1 Study Rationale.....	23

3.2 Meta-Analysis of Large Publicly Available Temporal Lobar Datasets Results in ApoE-Dependent Transcriptomic Signatures of Disease.....	23
3.3 Ontological Analysis Uncovers Disparate Pathways in ApoE-Specific Disease Signatures.....	24
Chapter 4: Bumetanide Ameliorates Cognitive, Electrophysiological, and Transcriptomic Deficits in ApoE4-KI Mice	26
4.1 Bumetanide Ameliorates the Learning and Memory Deficits in a Mouse Model of ApoE4-Mediated AD.....	27
4.2 Bumetanide Treatment Rescues Neuronal Plasticity and Excitability Deficits in a Mouse Model of ApoE4-Mediated AD.....	28
4.3 Bumetanide Recapitulates the Anti-Correlation of the Transcriptomic Signature of ApoE4-Mediated AD in the Mouse Hippocampus.....	29
Chapter 5: Discussion and Conclusion	46
Chapter 6: Future Directions	49
References	52

LIST OF FIGURES

Figure 1: ApoE-Genotype-Specific Transcriptomic Signatures of AD.....	31
Figure 2: ApoE-Genotype-Specific Drug Repositioning Analysis Identifies Bumetanide as the Top Predicted Drug Candidate for ApoE4/4 AD.....	32
Figure 3: Bumetanide Treatment Rescues Spatial Memory Deficit Specifically in Aged ApoE4-KI Mice.....	34
Figure 4: RNA-seq Analysis of the Transcriptomic Perturbation Signature of Bumetanide in the Hippocampus of apoE4-KI Mice.....	36
Supplementary Figure 1: Bumetanide Treatment Does Not Affect Swim Speed or Visible Trial Performance	39
Supplementary Figure 2: The Effects of Bumetanide Treatment in Wildtype Mice.....	40
Supplementary Figure 3: Variance Stabilizing Transformation Deviates from Log2 Transformation Only at Lower Values.....	41
Supplementary Figure 4: Principal Component Analysis of GSE15222 Dataset Reveals No Clustering Trend Across ApoE4 Genotype, Diagnosis, Age or Sex Covariates.....	42
Supplementary Figure 5: Principal Component Analysis (PCA) of the Syn3157255-MayoRNASeq Dataset After Batch Correction Reveals No Clustering Trend Across ApoE4 Genotype, Diagnosis, Age or Sex.....	43
Supplementary Figure 6: Data Integration by Probe Selection and Batch Correction Yields Normalized Dataset for Meta-Analysis.....	45

LIST OF TABLES

Supplementary Table 1: Covariate Measures for Human Transcriptomic Datasets.....	38
---	-----------

CHAPTER 1: INTRODUCTION

Alzheimer's Disease and ApoE4 Alzheimer's disease (AD) is the leading cause of dementia worldwide, with over 40 million people currently suffering from this neurodegenerative disease and no disease-altering therapies available.^{4,9,10} Neuropathologically, AD is characterized by the buildup of extracellular A β plaques and intra-neuronal neurofibrillary tangles of the protein tau¹⁰. Familial early onset AD has been linked to mutations of several genes in the amyloid processing pathway, initially implicating A β as a key player in AD pathology. These early onset cases, however, only account for approximately 1% of the AD population.^{6,10-12}

Early efforts to develop disease-modifying therapeutics for AD have been unsuccessful due to the poorly-understood multifactorial etiology of the disorder¹⁰. Since its characterization in the early 1900's, A β and tau have been extensively studied as drug targets.^{9,13} A β is a by-product of the cleavage of the APP protein with no known physiological function(Tan). Several promising compounds have been developed which successfully target all aspect of A β production, deposition and clearance, however none of these compounds have been efficacious in human clinical trials, suggesting that amyloid may not in fact be a driver of this disease.^{14,15} These costly failures have continually been attributed to the time point of treatment, however the causative versus compensatory nature of amyloid buildup during AD pathology is hotly contested.^{14,16}

The majority of AD patients (>98%) do not have a mutation in the APP/ A β processing pathway and develop symptoms anyway.^{4,9,10} They fall into the category of late-onset AD or LOAD, and 60-80% of them have a mutation in the apoE4 gene.^{4,9,10} ApoE4 was identified by epidemiological studies and GWAS as the greatest common genetic risk factor for late onset AD. The apoE locus has three naturally alleles in humans, apoE2, apoE3 and apoE4. ApoE4 incurs a 2–4 fold risk of AD for heterozygote carriers (~25% of the population) and a 12–14 fold risk for

homozygotes (~2% of the population) as compared to the neutral apoE3 allele.^{6,11,12,17} ApoE2 isoform is thought to be protective against cognitive decline, A β plaques in apoE4 carriers do not significantly correlate to regional functional deficits or cognitive decline, and longitudinal studies have identified cognitive changes in apoE4 carriers before the age of 30, indicating that this risk allele has detrimental effects on cognition independent of A β .¹⁰ (Haung Dennis, Fillipini).

While the mechanism of action of this risk allele is still actively under research, it is believed that it acts through A β -independent mechanisms⁵. There are several lines of evidence that support this hypothesis. Firstly, apoE4 is correlated with the reduction of glucose metabolism in the brain in individuals who are between 20 and 39 years old, prior to the onset of A β deposition.¹⁸ Secondly, studies have found that apoE4 and not A β , causes reduced glucose metabolism during normal aging.¹⁹

The effects of apoE4 in AD are multifactorial, with the allele impairing neuronal plasticity, adult neurogenesis, mitochondrial function, and stimulating tau phosphorylation.^{20,21} While the mechanism of action of this risk allele is still actively under research, it is believed that it acts through A β -independent mechanisms.^{5,10} ApoE4 differs from apoE3 by only one amino acid, but this causes a large conformational change in the protein which renders apoE4 much more vulnerable to proteolytic cleavage.^{4,20} The cleaved fragments of apoE4 are thought to be neurotoxic and play large role in the neurodegeneration in apoE4-mediated AD^{9,20}. ApoE4 is thought to enact pathology through tau, and therefore works in concert with the known pathological hallmarks of the disease.²²

ApoE4 has been extensively studied in a few transgenic mouse lines, the most prolific of which are mice with the human apoE3 or apoE4 gene knocked in to the endogenous mouse apoE locus.

ApoE4 knock-in female mice show significant deficits in learning and memory as measured by the Morris Water Maze by 16 months of age as compared to apoE3 controls.^{22,23} This is consistent with data showing that in humans, females are at higher risk for disease than males.^{6,11,12} These mice lose excitatory/inhibitory balance in the hippocampus due to the death of somatostatin positive inhibitory interneurons, and exhibit a marked decrease in dendritic spine density of hippocampal granule cells.²³⁻²⁵ These data, among the continued failure of costly clinical trials targeting A β , underscore the pressing need to develop unconventional drug development strategies that identify pathways and compounds to efficaciously treat AD.^{14,26}

1.2 Disadvantages of Pathway Based Drug Development Efforts

Four drugs have been approved in the U.S. for AD for symptom management, none of which slow disease progression.²⁷⁻²⁹ Three acetylcholinesterase inhibitors (donepezil, rivastigmine and galanthamine) are licensed for mild to moderate AD, and the NMDA receptor antagonist memantine is licensed to treat moderate to severe AD.²⁷⁻²⁹ While these drugs have been shown to improve cognition for a short period of time, there is a pressing need to develop therapies that slow disease progression.²⁷⁻²⁹ Drugs developed to combat the creation and accumulation of A β have had no effect in humans.^{4,14} The reasons for these high-profile failures are multifactorial. The amyloid pathway may not be the causative agent in advancing AD pathology, and these trials have been geared mostly towards mild to moderate AD patients, which may be too late in the disease progression for a therapy to be effective.²⁹

Unfortunately, several candidate therapies advanced to Phase III trials without adequate proof of concept of the mechanism of action. For example, the proposed mechanism of action of terenflurbil and semagacestat included modulation of the amyloid cleaving enzyme gamma-secretase, and the relative benefit of this modulation of the amyloid pathway and on AD disease

progression has not been confirmed,²⁶ leading to failed Phase III trials. Similarly, a distinct mechanism of action for dimebon was not known, and the magnitude of the impact of this drug on disease was minimal, with more expensive and unsuccessful Phase III trials.²⁶ Because of this, alternative drug targets are actively being sought out, including apoE4-related pathology.

1.3 Precision Medicine, Disease Modelling, and Alzheimer’s Disease:

Due to the complex genetics of AD pathology, precision medicine — the integration of prior knowledge of genetic variability into experimental design — has been shown to be paramount to successfully identifying mechanisms of disease.^{4,9,10,30} The integration of apoE genotype information with the analysis of transcriptomic data in the context of drug repositioning is an extremely powerful tool for the identification of efficacious drugs in AD.^{27,31-33} Furthermore, the multifactorial nature of apoE4-mediated AD pathology suggests that the application of a combinatorial drug approach may be required for efficacious treatment regimens.¹⁰ Precision medicine leans away from the traditional “one-size-fits-all” approach to drug discovery, instead pioneering the idea that each individual’s disease comes from a unique genetic milieu and while it may present with similar symptoms and pathology, is never the exact same pathological process and should not be treated as such.³⁴

While some fields such as anti-cancer efforts have benefitted enormously from precision medicine approaches, others, such as neurodegenerative diseases, are only in their infancy. This discrepancy stems from several factors. Firstly, access to large-scale biological tissue banks for brain tissue associated with neurodegenerative disease has been notoriously difficult. Only recently have such consortia as the NIH’s Accelerating Medicines Partnership – Alzheimer’s Disease (AMP-AD) been founded to pool together ‘omics data from brain tissue, and has spawned several high-profile papers despite its mere six years of existence.³⁵⁻³⁷ Secondly, the oft-used

mouse models of Alzheimer's Disease are notoriously biologically irrelevant.³⁸ Most mouse models rely on introducing 2-5 exceedingly rare autosomal dominant mutations in the amyloid processing pathway which have never naturally occurred in tandem in humans, causing a massively overstated and precocious amyloid phenotype leading to early cognitive impairments and amyloid pathology in the mouse brain.³⁸ Most of the failed clinical trials over the last ten years, of which there have been many, have developed anti-amyloid compounds that while effective in mice, are ineffective if not detrimental in humans.²⁶ The inability and/or reluctance of large pharma to move away from these highly erroneous mouse models has not only cost billions of dollars but has led to the loss of countless lives as the search for therapies remains stymied in clinical trials. The canonical "loudest voice wins" model of rigorous scientific rebuttal has created a self-aggrandizing community of amyloid enthusiasts who have unabashedly continued to shut down dissenting, and in this case, accurate, scientific voices to create an affirmation bubble of the most dangerous variety.

The theory of precision medicine when applied to the field of AD allows for the possibility for the 1% of AD patients that have an autosomal dominant amyloid mutation to potentially be experiencing a symptomatically similar but biologically distinct disorder from those with sporadic or apoE4-derived pathologies.^{10,34} While presenting with similar symptoms of spatial learning and memory impairment, the underlying generator of cognitive decline is most likely quite distinct and amyloid independent.^{4,10} This simple yet revolutionary idea has only recently taken a foothold among government funding agencies, which have slowly been shifting their support away from the ongoing amyloid apocalypse as more and more amyloid-related clinical trial failures unfold across the world.

1.4 Drug Repositioning in AD Drug Development.

The pathobiology of the apoE4 risk allele remains poorly understood, significantly hindering the classical one-target approach to drug development.^{5,9,30} Drug repositioning, a computational method for predicting new uses for FDA approved compounds offers less drug development costs and shorter paths to approval for clinical use.^{39,40} Drug repositioning has been used successfully in such areas as cancer, cardiovascular disease, irritable bowel syndrome, obesity, erectile dysfunction, smoking cessation, psychosis, attention deficit disorder and Parkinson's disease.⁴¹⁻⁴⁸ Because the compounds have an established safety profile in humans, they have several advantages over conventional drug development strategies.^{31,39,40,49}

Developing new drugs to combat disease is an arduous and incredibly high-risk process. Each new drug that makes it through the FDA can take on the order of 10-15 years and two billion dollars to be approved, with a success rate of only 2%.⁴¹ Because of this, the rate of drug approvals has been steadily declining since 1995.⁵⁰ Investment in new drug development has been gradually decreasing in a similar manner indicating that the cost of new drug development will continue to skyrocket.⁴¹ This combined with the steadily growing population with Alzheimer's disease creates a dire need for the quick development of new therapeutics.

The concept of drug repositioning, or the repurposing of already FDA-approved drugs for innovative uses, is not new. In fact, several of the most lauded successes of the 20th century were due to serendipitous accidents whereby a drug approved for one indication was found to be effective in an entirely different disease. Thalidomide, for example, was originally developed as a sedative, but after its disastrous effects on pregnancy were discovered, clinicians realized it had potent anti-cancer properties.⁵¹ Traditional drug development pipelines include discovery and

pre-clinical, safety review, clinical research, FDA review, and FDA post-market safety monitoring.⁵⁰ Repurposed drugs on the other hand, have already received FDA approval, making the journey to the clinic much faster.

In the past decade, the amount of publically pharmacological data has grown exponentially, vastly reducing the need for drug development pipelines to be developed from the ground up. A variety of wet lab and computational approaches have been developed to discover new drug-disease relationships. A plethora of drug and disease knowledge databases have been developed including DrugBank, ChemBank, the Therapeutic Target Database, PharmGKB, and PubChem, to name a few.⁵²⁻⁵⁵ Simultaneously, such public genomic repositories such as GenBank, GEO, and AMP-AD allow for the gathering of large phenotypic disease datasets for in silico drug testing. The work presented in this thesis ascribes to the network based approach to drug repositioning, whereby a drug is matched to a disease based on its gene network perturbation. The underlying premise of this approach is that every drug has a gene network effect, and that “side-effects” are rather a phenotyping expression of a drug’s perturbation network.

1.5 The Connectivity Map and Pharmacogenomics:

The Connectivity Map (CMAP) database is a resource which consists of transcriptomic profiles of 1309 diverse bioactive compounds in 5 different cell lines as compared to untreated controls, of which nearly 800 have FDA approval status.^{8,32} This resource, among others, has recently opened up the possibility of a systems approach to drug discovery. Genetic perturbations in human disease are contrasted with that of a compound’s perturbation profile in cell lines to find drugs that best anti-correlate, or “flip” the genetic signature of human disease back to that of

control tissue.^{8,31,56} This method has been continually validated in several human diseases but has been applied but not yet been successfully validated in AD.^{31,35,57,58} The Connectivity map (Cmap) was created by Lamb et al., in 2006.⁸ The authors introduced a database that attempts to describe all biological states in terms of genomic signatures, producing a resource that could be mined for pattern-matching between drug and disease perturbations.^{8,50} Since the publication of this resource, other such databases such as LINCS, Cytoscape, K-map, and Dt-web have been introduced, further enhancing our understanding of the triad of genes, drugs and disease.⁵⁹⁻⁶² These methods have all given rise to novel drug-disease relationship hypotheses that have proven to translate to having a therapeutic in in vivo animal models and even in the clinic.⁶³

CMap and its more comprehensive predecessor LINCS and ssCMAP are most often used to map global network drug and disease signatures, and therefore does not require detailed knowledge of a mechanism of action (MoA) in order to predict therapeutic agents.^{8,60} In diseases such as Alzheimer's disease where the MoA is unknown, this presents a giant leap forward for therapeutic research.^{31,33,40} In the past decade, these big-data resources such as the CMap and LINCS among others have been used extensively to map drugs to disease and vice-versa, however the true power of these methods has yet to be unlocked as we continue into an era of ever bigger data and computational power.

1.6 Methods of Drug Repositioning

Since its introduction in 2006, the CMap has been used extensively across diseases to predict new drug-disease relationships. The canonical use of this resource involves one of three methods: a) Using gene expression signature changes in disease states as a search tool across drug perturbagen profiles, b) using drug-to-gene network data to identify chemicals with similar

expression patterns and therefore potentially similar mechanisms of action, and c) for drug combination research.^{39,49,64} As a tool to elucidate new therapeutic mechanisms, the CMap has been used successfully to discover novel therapeutic agents in CNS injury, glioma, Gaucher disease, ovarian cancer, leukemia, prostate cancer, Diabetes, among other diseases.⁶⁵⁻⁶⁹ CMap has also been employed to investigate the relationship between drugs and microRNAs, as well as drug-drug interactions and pairwise combinations of compounds for therapeutic use across diseases.⁷⁰⁻⁷²

The central thesis of drug repositioning is that all drug act in a gene network-based manner, summarily excluding the one drug-one target approach to therapeutic development. The mechanism of action of a drug, therefore, can be understood as the sum of its effects across the entire gene-gene and protein-protein interaction network. In this vein, the CMap can be applied to better understand the full mechanism of action of a drug in a biological system, in this case, the cell.^{8,69,73,74} The CMap and other computational drug databases have been employed to better understand basic drug-disease relationships, and to elucidate previously misunderstood mechanisms of action, and to find drug-able targets and their corresponding therapeutic compounds that existed outside the scope of previous scientific understanding.⁷⁴ Techniques have been developed to modeling functional protein interaction networks, investigating potentially therapeutic ‘side effects’, and uncovering more comprehensive information about known targets and the gene network pathways within which they exist.^{43,68,73}

1.7 Bumetanide as a Repurposed Therapeutic Compound

In this thesis, I demonstrate that bumetanide can be repurposed to ameliorate the learning and memory deficits in apoE4-mediated AD. Bumetanide is an FDA-approved small molecule

currently used to treat edema, usually after heart, liver or kidney failure.⁷⁵⁻⁷⁹ It's canonical mechanism of action is as an inhibitor of the sodium-potassium-chloride transporter NKCC1 and the kidney-specific NKCC2.⁸⁰ Bumetanide changes the osmotic balance in the loop of Henle in the kidney, causing acute diuresis for patients with edema.^{81,82} In 1997, McGahan et al., demonstrated that Bumetanide targets NKCC1 *in vitro* and reduces influx of chloride into the cell without changing chloride outflux, and that the transport of sodium and potassium ions across the membrane was heavily reduced.⁸³ Haas and McManus had previously shown that by changing the chloride concentration they could shift the dose-response curve for bumetanide suggesting that bumetanide was a competitive inhibitor of NKCC1.⁸⁴ NKCC1 knockout mice are immune to the effects of Bumetanide, further leading to the current understanding of the canonical mechanism of action of this drug.⁸⁵

Bumetanide has also been shown to change chloride homeostasis in neurons *in vitro* in slice recordings in the pyramidal cells of the hippocampal regions CA1 and CA3.^{85,86} These slice recordings found that application of bumetanide causes a hyperpolarization of neurons, making them less susceptible to excitotoxicity associated with overactivity.⁸⁷ Due to its known inhibitory effects, bumetanide has been studied as a potential therapy for epilepsy, Down syndrome, Parkinson's disease, autism, and schizophrenia.^{85,88-90} Bumetanide is a strong inhibitor of NKCC1, with a half-maximal concentration (IC₅₀) of 100-500nM, however it has a relatively short half-life (~1 hour in humans and ~30 minutes in rodents) and is not very bioavailable with a 1:100 brain:plasma ratio.^{75,91-94} Despite these pharmacogenetic properties, doses as low as 0.2 mg/kg bumetanide administered systemically have been shown to have disease-modifying effects in mouse models of acute seizure.^{88,95}

1.8 Research Purpose

In the search for better therapeutic agents against AD pathologies, we sought to apply precision medicine techniques to screen the CMap to screen for potential small molecule candidates in an apoE-dependant manner. We demonstrate that bumetanide is predicted to be efficacious against apoE4-mediated disease and we validate our findings in an apoE4-KI mouse model of disease.

CHAPTER 2: MATERIALS AND METHODS

2.1 Data Integration.

GEO and AMP-AD were searched for transcriptomic AD data from temporal lobe tissue for which apoE genotype information was available. Microarray experiments from Webster et al., 2009⁹⁶, accession GSE15222, was downloaded directly from the NCBI GEO database⁹⁷ in the available series matrix file format. Data had been rank-invariant normalized as described^{96,98}. The pre-normalization procedure created negative values in the series matrix file, which were eliminated by adding a constant across the expression matrix⁹⁹. Since fold change (FC) calculated after this addition is an underestimation, all subsequent FC estimates are conservative relative to the stated thresholds. Log2 transformation was then applied to the all-positive-value expression matrix. All samples with an apoE3/3, apoE3/4, or apoE4/4 genotype were used for further analysis except one sample with no reported gender. The Syn3157255-MayoEGWAS dataset was downloaded from the AMP-AD portal. The data had been background corrected and subjected to variance stabilizing transformation (Vst), quantile normalization, and probe filtering with the lumi package of BioConductor, as described¹⁰⁰. Vst is identical to log2 transformation at higher values, but deviates at lower values (Supplementary Fig. 2)¹⁰¹. The Vst algorithm results in underestimation of FC values of Vst transformed data calculated based on a log2 scale under this deviation value. Thus, subsequent FC estimates for this dataset were also conservative relative to the stated thresholds.

Both datasets were analyzed by principal component analysis (PCA) to confirm normalization of technical artifacts (Supplementary Figs. 3 and 4). Since such artifacts were present in the first principal component, the Syn3157255-MayoEGWAS dataset was further batch corrected across the “plate” covariate by using the ComBat function of the sva package¹⁰². The Limma R package, which uses linear models for differential expression (DE) analysis, was applied to each dataset

separately to estimate DE of genes in all control and AD samples regardless of apoE genotype; for genes with more than one probe, the probe with the most significant P value for the difference between AD and control samples was used for subsequent integration and meta-analyses of the two datasets¹⁰³. Both datasets were separated into apoE-genotype-specific groups (apoE3/3, apoE3/4, and apoE4/4); genes shared by both microarray platforms (16477 genes) were batch corrected across the two datasets for each group with the ComBat algorithm (sva package) (Supplementary Fig. 5).

2.2 Differential Expression and Pathway Analysis.

Average age did not differ in apoE genotype groups, except in the apoE3/4 AD group, which was higher in the Syn3157255-MayoEGWAS study (+3.24 years, ANOVA with Tukey HSD post-hoc testing, $P = 0.0153$). To maintain power, no samples were removed from the apoE3/4 group in Syn3157255-MayoEGWAS. To ensure that age did not affect our DE results, we calculated the Pearson's correlation of the expression level in the Syn3157255-MayoEGWAS dataset of each DE gene from both the apoE3/4 control and AD datasets against the age covariate. No genes correlated significantly ($FDR < 0.05$). To eradicate any spurious results related to non-sex-matched groups, each apoE-genotype-specific groups were randomly down-sampled to match the male to female ratios within each genotype across diagnoses (Supplementary Table 1). To account for possible stochastic effects, this process was applied 10 times. The nonparametric rank-based algorithm RankProd (version 2.42.0) was applied to each of the 10 permutations with a two-origin design. The two-origin design RankProd algorithm computes pairwise FC ratios for every control and AD sample in each dataset separately, ranks the ratio of each gene within each pairwise comparison, and calculates the rank product of each gene by taking the product of all pairwise rank

ratios from both datasets. *P* values were determined by 1000 permutations¹⁰⁴. Adjusted *P* values were determined separately with the *p.adjust* base function in R. The ComBat function changes the mean and SD of each sample. Therefore, to avoid further artifacts in the reported FC estimation by the RankProd package, FCs used in all subsequent cutoffs were calculated separately for each dataset before batch correction, and the arithmetic mean was used. Because of the normalization transformations of the GSE15222 matrix and the Vst transformation of Syn3157255-MayoEGWAS, some FC values are underestimated and are referred to as “estimated FC”. Estimated FC values and *P*-values were averaged over each of the 10 sex-matched permutations for each genotype and FDR values were calculated using the *p.adjust* package. DE genes that had both an estimated average absolute FC greater than 1.3x and an FDR cutoff < 0.05 were further analyzed. DE genes of drug signatures were analyzed with Ingenuity Pathway Analysis (IPA) software. Ontology analysis was done using the reference set from the Ingenuity Knowledge Base including direct and indirect gene relationships; enrichment *P*-values were taken directly from the IPA software.

2.3 Drug Repositioning Analysis.

The computational drug repositioning algorithm, which was developed by Sirota et al. and Dudley et al.^{41,42} and taken from Chen et al.⁴⁴, was applied to each apoE-genotype-specific gene signature using the publically available CMap database (1300 compounds). Although LINCS is a much more comprehensive database, only a very small proportion of DE genes in AD overlapped with the 1000 genes measured, and therefore it was not used in this study. The algorithm was modified to use the full apoE-genotype-specific DE signature rather than the top 150 up- and downregulated genes. FDR-adjusted *P* values were calculated with the *p.adjust* function in the

base R package. Technical replicates, defined as the same drug, concentration, cell line, and treatment, were averaged by CMap score. In the analysis of overlapping drug predictions between apoE-genotype-specific groups, when drugs had more than one technical replicate, the *P* value from the most significant replicate was reported in order to have the most inclusive drug set. The cell line with the lowest CMap score was reported for each compound to further enrich the signal. The raw CMap data for bumetanide in PC3 cells was extracted for further analysis. The CMap data from the pipeline detailed by Chen et al.⁴⁴ consists of the FC rank after bumetanide treatment. To display how bumetanide “flips” the apoE4/4-specific transcriptomic signature of AD, the CMap data in Figure 2 were analyzed by Monte Carlo simulation to calculate the significance of the shift in the average FC rank. Downregulation by bumetanide was defined as a shift of upregulated apoE4/4 human gene signatures to a lower rank than the mean rank of all genes. Upregulation by bumetanide was defined as a shift in average FC rank of the downregulated genes in the apoE4/4-specific AD signature toward a higher rank than the mean rank of all genes.

2.4 Mice.

All protocols and procedures followed the guidelines of the Laboratory Animal Resource Center at the University of California, San Francisco (UCSF). All mice were housed under identical conditions from birth through death (12-hour light/dark cycle, housed 5/cage, PicoLab Rodent Diet 20). All mouse lines were maintained on a C57Bl/6J background. ApoE3-KI and apoE4-KI homozygous mice (Taconic)^{105,106} as well as wildtype mice were born and aged under normal conditions at the Gladstone Institutes/UCSF animal facility. Female apoE-KI mice were used because of their susceptibility to AD-related neuronal and behavioral deficits. Gender-matched

wildtype mice were used as controls. The ages of the mice are indicated in the behavioral testing section of the online methods.

2.5 Bumetanide Treatment.

Bumetanide was prepared at 220 μ M in 2% DMSO in 0.9% sterile saline, adjusted to pH 8.5 with NaOH for solubility, and given by i.p. injection daily to apoE-KI and wildtype mice, starting 6 weeks before and continuing throughout behavioral assessment. Body weight was measured weekly during bumetanide treatment; injection volume was calculated to achieve a dose of 0.02 (low) or 0.2 (high) mg bumetanide/kg body mass (e.g., 50- μ l daily injection for a 20-g mouse). Control mice were injected with a matched volume of 2% DMSO in 0.9% sterile saline, pH 8.5. Injections were well tolerated and had no adverse effects on health.

2.6 Behavioral Testing.

Mice were singly housed before testing. Each mouse was assigned a random number, so researchers were blinded to genotype and treatment information. At about 14 months of age, apoE3-KI and apoE4-KI mice were randomly assigned to treatment groups: apoE3-KI vehicle (n = 10, age 14.01 \pm 0.44 months), apoE3-KI low bumetanide (n = 11, age 14.30 \pm 0.33 months), apoE3-KI high bumetanide (n = 10, age 13.74 \pm 0.22 months), apoE4-KI vehicle (n = 10, age 14.10 \pm 0.35), apoE4-KI low bumetanide (n = 10, age 14.70 \pm 0.27 months), apoE4-KI high bumetanide (n = 9, age 13.77 \pm 0.28 months), wildtype vehicle (n = 16, age 16 months), wildtype bumetanide (n = 15, age 16 months). Treatment was administered daily by i.p. injection beginning 6 weeks before and continuing throughout the 14 days of testing in the Morris water maze (MWM); injections were given at the end of the light cycle and after the day's test.

The MWM pool (diameter, 122 cm) contained opaque water (22–23°C) with a platform 10 cm in diameter. The platform was submerged 1.5 cm during hidden platform sessions^{23,107-110} and marked with black-and-white-striped mast (15 cm high) during cued training sessions. Mice were trained to locate the hidden platform (hidden days 1–5) and the cued platform (visible days 1–3) in two daily sessions (3.5 h apart), each consisting of two 60-s trials (hidden and cued training) with a 15-min intertrial interval. Distal visual cues on the walls of the behavioral testing room remained constant throughout the test. Visible trials took place after training and memory probes and were 60 seconds long with a cued visible platform. The platform location remained constant in the hidden platform sessions but was changed for each cued (visible) platform session. Entry points were changed semirandomly between trials. At 24, 72, and 120 hours after the last hidden platform training, a 60-s probe trial (platform removed) was done. The entry points for the probe trial was in the southwest quadrant, and the target quadrant was the northeast quadrant. Performance was monitored with an EthoVision video-tracking system (Noldus Information Technology). For the probe trials, we analyzed (1) the percent time spent in the target quadrant versus average time spent in the three other quadrants, (2) the number of crossings over the position of the target platform versus the average number of crossings over the equivalent positions in the three other quadrants and (3) the distance to platform over the first 10 seconds.

2.7 RNA-Seq Analysis of Hippocampal Tissue.

Twelve-month-old apoE3-KI and apoE4-KI mice received daily i.p. injections of vehicle or bumetanide (0.2 mg/kg body weight) for 60 days. Mice were perfused with 0.9% saline, and the hippocampus was dissected and homogenized in Trizol reagent. Total RNA was extracted and purified with the Qiagen RNeasy Micro kit, which included a DNase treatment. cDNA was

generated from full-length RNA (50 ng per sample) with the NuGEN RNA-Seq V2 kit, which uses the single primer isothermal amplification method to deplete ribosomal RNA, and sheared by Covaris to yield fragments of uniform size. The NuGen Ultralow system V2 was used for adding adapters and for barcoding and amplification. The resulting RNA libraries were purified with Agencourt XP magnetic beads, and quantified by qPCR after quality control with an Agilent Bioanalyzer. The libraries were pooled and sequenced with a HiSeq 4000 instrument (Illumina) for single-end (SE50) sequencing. Sequence data were aligned with the STAR short read aligner¹¹¹ and counts per feature were obtained with the featureCounts function from the Subread package¹¹². After alignment, transcripts not shared in the GSE15222 and Syn3157255-MayoEGWAS databases were discarded, as were genes with less than one count per million in two or more samples¹¹³.

The DESeq pipeline was used to assess DE of the remaining 11,877 transcripts. Genes below a *P* value of 0.05 were considered DE for future pathway analysis. After count normalization with DESeq, data were rld transformed (vsn package), and clustering was done on the DE genes with the pheatmap package. PCA was applied to the rld-transformed DE genes. The DE signatures of drugs were analyzed with Ingenuity Pathway Analysis software. Ontology analysis was done using the reference set from the Ingenuity Knowledge Base including direct and indirect gene relationships. For analysis of rank changes of apoE-genotype-specific signature genes of AD, the raw count data from the 11,877 transcripts were rank transformed, and for each gene the average rank of vehicle-treated samples was subtracted from that of bumetanide-treated samples. Significance of the rank changes of the up- and downregulated apoE4-KI human gene signatures deviating from the population mean of the rank change of all genes (zero) was calculated by Monte Carlo simulation.

2.8 Brain Slice Electrophysiological Recordings and Data Analyses.

ApoE4-KI mice were randomly allocated to vehicle ($n = 3$, age 15.2 ± 0.85 months) and control ($n=3$, age 15.1 ± 0.06) groups. ApoE3-KI mice were similarly allocated into vehicle ($n=3$, age 15.5 ± 0.17) and control ($n=3$, age 15.57 ± 0.29) groups. Mice were dosed from 4 – 6 weeks and slice recording day / dosage time were allocated randomly between the groups to allow for equal dosage time while experiment was performed. At time of recording all mice were approximately 16 months of age.

2.9 Statistical Analyses. Behavior metrics are expressed as mean \pm SEM. All values for n are the numbers of mice or biological replicates. The distribution of data was assessed with the Shapiro-Wilk normality test; most of the data were normally distributed. Differences between groups were determined by unpaired or paired two-sided t test. For multiple comparisons, one-way ANOVA and Tukey's post-test were used. $P < 0.05$ was considered significant. Researchers were blinded to genotypes and treatment information during experiments.

2.10 Compliance with Relevant Ethical Regulations and Animal Use Guidelines. All experimental and animal protocols and procedures were done in accordance with the university and institutional ethical regulations and animal use guidelines.

**CHAPTER 3: BUMETANIDE IS PREDICTED TO BE EFFICACIOUS AGAINST
APOE4-MEDIATED AD**

3.1 Study Rationale

The patient heterogeneity of AD caused by different genetic, epigenetic, and environmental factors suggests that attempting to develop a single drug suitable for all AD patients may be a severe over-simplification. Consequently, the combination of precision medicine guided by disease-associated gene mutations or polymorphisms with computational drug repositioning might be an alternative approach to identify existing drugs effective for subpopulations of AD patients. Our drug repositioning approach for AD builds on the well-validated hypothesis that drugs which perturb or “flip” differentially expressed (DE) genes in a disease state back towards control levels may be efficacious against this disease^{41-43,114-117}. Within this pipeline, the first step is to establish apoE-genotype-specific transcriptomic signatures of AD. The second is to apply a validated computational drug-repositioning algorithm⁴¹⁻⁴⁴ to query the CMap database, which contains transcriptomic perturbation signatures of 1300 drugs⁸. Each compound receives a prediction score for therapeutic potential in apoE-genotype-specific AD^{41,42,44}; a negative score suggests that a compound might reverse the transcriptomic signature of the disease. Since transcriptomic signatures of AD are compared with those perturbed by each compound, the prediction strategy is driven by the DE gene signature of the disease rather than by a hypothesis-driven approach targeting isolated pathways. Finally, the top predicted drug is tested in a mouse model of apoE4-driven AD to validate efficacy and explore mechanisms of action.

3.2 Meta-Analysis of Large Publically Available Temporal Lobar Datasets Results in ApoE-Dependent Transcriptomic Signatures of Disease

To establish apoE-genotype-specific transcriptomic signatures of AD, we analyzed the two largest public human temporal lobar transcriptomic datasets with apoE-genotype information—

GSE15222 (n = 213)⁹⁶ and Syn3157255-MayoEGWAS (n = 397)¹⁰⁰ (**Fig. 1a, Supplementary Table 1**). As in most clinical studies⁶, AD groups in each dataset had proportionately more apoE3/4 and apoE4/4 carriers than controls (**Fig. 1b**). The datasets were stratified by apoE genotype for meta-analysis (**Fig. 1a**) using a nonparametric algorithm, RankProd¹⁰⁴. Genes with an average false-discovery rate (FDR)-adjusted *P* value < 0.05 and an average absolute estimated fold change (FC) > 1.3x were further analyzed. Comparison with apoE-genotype-matched controls showed up- or down-regulation of 314, 150, and 696 genes in AD subjects with an apoE4/4, apoE3/4, and apoE3/3 genotype, respectively (**Fig. 1c,d, Supplementary Tables 2–4**). Strikingly, only 31 DE genes (2.7% of all DE genes) were shared among all three AD groups (**Fig. 1c,d, Supplementary Tables 2–4**), highlighting the unique pathobiology of each apoE genotype in AD pathogenesis.

3.3 Ontological Analysis Uncovers Disparate Pathways in ApoE-Specific Disease Signatures

Ontological analysis identified 28, 24, and 48 perturbed pathways in apoE4/4-, apoE3/4-, and apoE3/3-specific signature of AD (**Fig. 1e, Supplementary Tables 5–7**). Only three (3% of all perturbed pathways) were shared among all three AD groups (**Fig. 1e, Supplementary Tables 5–7**), further highlighting the unique effect of each apoE genotype on the molecular milieu of AD. Next, we applied the apoE-genotype-specific transcriptomic signatures of AD to the CMap database to produce therapeutic predictions⁴⁴. The FDA-approved loop-diuretic bumetanide had the best predictive score against apoE4/4 AD (**Fig. 2a**, see Online Methods for detailed analytic procedures) and a much weaker CMap score against apoE3/4 and apoE3/3 AD (**Fig. 2b,c**). In bumetanide-treated cells in the CMap database, genes upregulated in apoE4/4 AD were shifted downward (higher rank numbers, *P* = 0.003 by Monte Carlo simulation) and those downregulated in apoE4/4 AD were shifted upward (lower rank numbers, *P* = 0.002 by Monte Carlo simulation)

(Fig. 2d–g), confirming that the transcriptomic perturbation signature of bumetanide correlates negatively with that of apoE4/4 AD.

CHAPTER 4: BUMETANIDE AMELIORATES COGNITIVE, ELECTROPHYSIOLOGICAL,
AND TRANSCRIPTOMIC DEFICITS IN APOE4-KI MICE

4.1 Bumetanide Ameliorates the Learning and Memory Deficits in a Mouse Model of ApoE4-Mediated AD

For *in vivo* validation, we examined the effects of bumetanide treatment at low (0.02 mg/kg) and high (0.2 mg/kg) doses (daily intraperitoneal injection for 8 weeks) on cognitive deficits in 16-month-old apoE4-KI mice. We used the Morris water maze (MWM)^{23,107-109} to test spatial learning and memory over 5 days in hidden platform learning trials followed by probe trials of short-term memory at 24 hours after the last hidden trial and long-term memory at 120 hours (**Fig. 3a**). Learning curve and swim speed did not differ across genotype or treatment groups during the hidden trials (**Fig. 3b**, **Supplementary Fig. 1a,b**). Bumetanide treatment did not alter learning curve and swim speed of wildtype mice either (**Supplementary Fig. 2a,b**). However, vehicle-treated apoE4-KI mice had impairment of short-term memory not seen in vehicle-treated apoE3-KI mice (**Fig. 3c**) and vehicle- and bumetanide-treated wildtype mice (**Supplementary Fig. 2c,e**). Strikingly, bumetanide treatment at both low and high doses rescued the short-term memory deficit of apoE4-KI mice, which performed as well as apoE3-KI mice, in the 24-hour probe trial (**Fig. 3c**). Low bumetanide- and vehicle-treated apoE3-KI mice performed equally well, suggesting that low dose of bumetanide treatment does not adversely affect memory formation. However, high dose of bumetanide treatment impaired short-term memory of apoE3-KI mice in the 24-hour probe trial (**Fig. 3c**), indicating the specificity of bumetanide's beneficial effect on apoE4-KI mice. In the 120-hour probe trial, high bumetanide-treated apoE4-KI mice still had a significant preference for the target quadrant (**Fig. 3d**), indicating a strong beneficial effect of bumetanide on long-term memory of apoE4-KI mice. Interestingly, either low or high bumetanide-treated apoE3-KI mice forgot the hidden platform location, like the vehicle-treated apoE3-KI mice, in the 120-hour probe

trial (**Fig. 3d**), again suggesting that the beneficial effect of bumetanide on long-term memory is specific for apoE4-KI mice.

In a more stringent test of spatial memory, we counted precise crossings of the target platform position versus similar areas in the other quadrants during each probe trial to assess the specificity and accuracy of memory performance. Strikingly, high bumetanide-treated apoE4-KI mice, but not apoE3-KI mice, had significantly more platform crossings in the target quadrant in both the 24- and 120-hour probe trials (**Fig. 3e,f**). Low bumetanide-treated apoE4-KI mice had a trend toward significant improvement of short-term memory accuracy in 24-hour probe trial (**Fig. 3e**). Interestingly, high bumetanide treatment impaired short-term memory accuracy in 24-hour probe trial (**Supplementary Fig. 2d**). Taken together, these data demonstrate that bumetanide restored the accuracy of both short- and long-term memory performance specifically in apoE4-KI mice.

4.2 Bumetanide Treatment Rescues Neuronal Plasticity and Excitability Deficits in Aged ApoE4-KI Mice

In an effort to gain a better understanding the underlying mechanisms of apoE4-specific behavioral rescue, we tested the genotype-specific effects of bumetanide on long-term potentiation (LTP). LTP is an electrophysiological measurement of neuronal plasticity²⁴. It has been considered as a molecular mechanism underlying normal memory formation²⁴, and it is impaired in animal models of AD²⁵. In line with memory impairment of aged (16-month-old) apoE4-KI mice, LTP recorded in the CA1 region of the hippocampal slices showed significant deficit in aged vehicle-treated apoE4-KI mice compared to age-matched vehicle-treated apoE3-KI mice (**Fig. 3, G and H**). Bumetanide treatment (0.2 mg/kg for 8 weeks) completely rescued LTP deficit in aged apoE4-KI mice (**Fig. 3, G and H**). Furthermore, neuronal hyperexcitability in the CA1 region of the

hippocampus in apoE4-KI mice, measured by input-output curve analysis²⁶, was also normalized by bumetanide treatment (Fig. 3I). Thus, *in vivo* bumetanide treatment restored neuronal plasticity and excitability, which underlies normal memory formation, in the hippocampus of aged apoE4-KI mice.

4.3 Bumetanide Recapitulates the Anti-Correlation of the Transcriptomic Signature of ApoE4/4-Mediated AD in the Mouse Hippocampus.

Finally, to explore bumetanide's effects on the transcriptome *in vivo*, we performed an RNA-seq analysis of the hippocampus, a temporal lobe region considered the epicenter of AD pathologies¹, from apoE4-KI mice treated with vehicle or bumetanide (0.2 mg/kg daily intraperitoneal injection) for 8 weeks. Hierarchical clustering and principal component analyses showed significant clustering of samples based on DE genes from bumetanide versus vehicle treatment (**Fig. 4a,b, Supplementary Table 8**), suggesting a distinct drug effect in the hippocampus. Furthermore, in bumetanide-treated apoE4-KI mice, the genes significantly upregulated in apoE4/4 AD were shifted down in their expression ranks (toward higher numbered ranks) (**Fig. 4c,d**, $P < 0.001$ by Monte Carlo simulation), corroborating the CMap data and the hypothesis that reversal of the disease-specific transcriptomic signature is a rational strategy for computational drug repurposing, even in animal models. However, in apoE4-KI mice, bumetanide did not alter the smaller subset of genes downregulated in apoE4/4 AD (**Fig. 4e**), perhaps because some of the downregulated genes reflect cell death rather than altered gene expression in apoE4/4 AD.

Pathway analysis of the genes whose expression was most affected by bumetanide in apoE4-KI mice ($P < 0.05$) identified 71 significantly perturbed pathways (**Supplementary Table 9**). Interestingly, six of these pathways overlapped with those enriched in the apoE4/4 AD signature:

GABA receptor signaling, cAMP-mediated signaling, G-protein-coupled receptor signaling, VDR/RXR activation, synaptic long-term depression, and CCR3 pathways (**Fig. 4f**). Future investigation is warranted to determine whether any of these perturbations are responsible for the beneficial effects of bumetanide.

Figure 1



Figure 1. ApoE-genotype-specific transcriptomic signatures of AD. (a) Experimental workflow, including dataset selection and integration, apoE genotype stratification, DE analysis of genes, drug repositioning analysis, and behavioral and transcriptomic validation. (b) ApoE genotype composition of AD and control datasets GSE15222 (n = 213) and Syn3157255-MayoEGWAS (n = 397). ApoE4 allelic representation (apoE3/4 and apoE4/4) was greater in AD groups (χ^2 test of apoE4 carriers versus non-carriers in AD versus control populations, $P < 0.001$). (c, d) Venn diagram of overlapping and unique upregulated (c) and downregulated (d) DE genes (Estimated absolute FC > 1.3x, FDR < 0.5) from apoE-genotype-specific, rank-based meta-analysis. 153 genes were uniquely significantly upregulated in apoE4/4 AD, 15 in apoE3/4 AD, and 319 in apoE3/3 AD. Only 18 DE genes were shared across these groups. 69 genes were uniquely significantly downregulated in apoE4/4 AD, 8 in apoE3/4 AD, and 193 in apoE3/3 AD. Only 13 DE genes were shared across all three groups. (e) Venn diagram of shared and unique significantly enriched ontological pathways across apoE-genotype-specific groups. Nineteen pathways were uniquely significantly enriched in apoE4/4 AD, 10 in apoE3/4 AD, and 28 in apoE3/3 AD. Only 3 pathways were shared across all three groups.

Figure 2

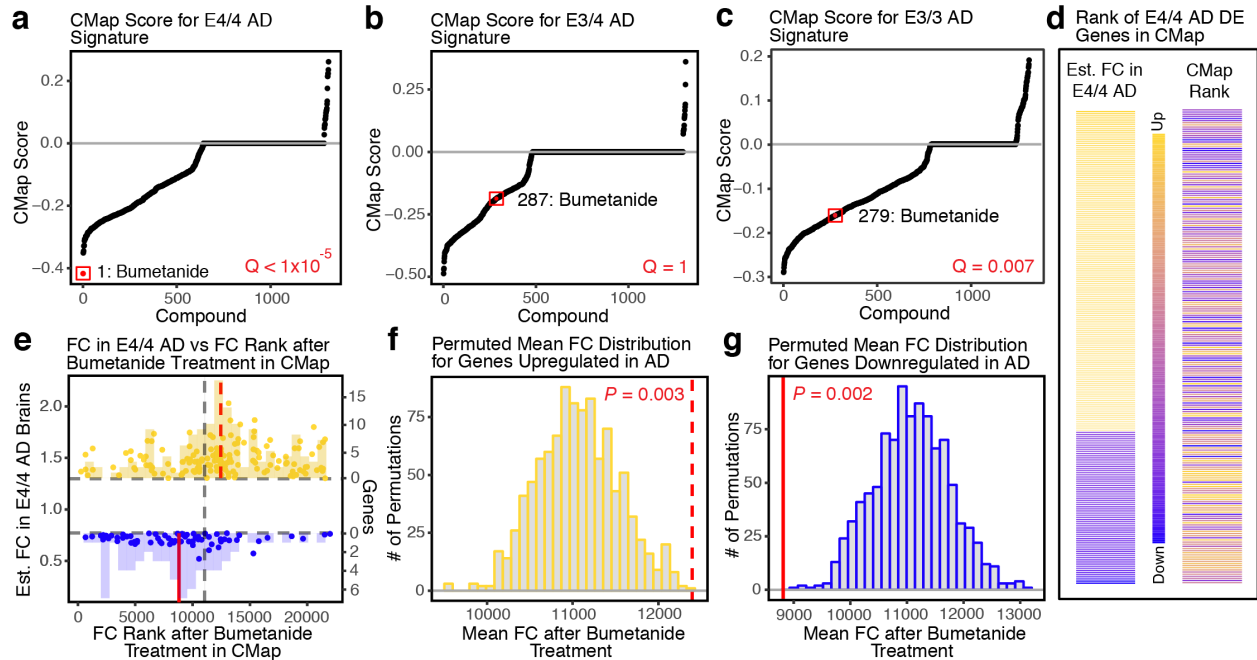


Figure 2. ApoE-genotype-specific drug repositioning analysis identifies bumetanide as the top predicted drug candidate for apoE4/4 AD. (a–c) Graphs of CMap compounds ordered by CMap score against (a) apoE4/4-specific, (b) apoE3/4-specific, and (c) apoE3/3-specific transcriptomic signatures of AD. While CMap score is negative for all three genotypes, adjusted p-value (Q) for the CMap score associated with bumetanide is significant for apoE4/4, as the top predicted drug, and apoE3/3 AD, but not for apoE3/4 AD. (d) Heatmap of genes from apoE4/4-specific transcriptomic signature of AD, rank ordered and color coded by estimated FC in apoE4/4 AD (left) and then re-color-coded by CMap rank (right). Bumetanide flips the expression rank of both up- and down-regulated genes in the apoE4/4-specific transcriptomic signature of AD. (e) FC rank from CMap data versus estimated FC of DE genes in apoE4/4 AD, as determined by rank-based meta-analysis (see Fig. 1 and Online Methods). Horizontal dotted lines indicate estimated FC cutoff of 1.3 (151 upregulated and 71 downregulated genes in the apoE4/4 signature of AD were shared in the CMap data). Mean FC rank of all genes after bumetanide treatment in the CMap data is 11,066.54 (vertical gray dotted line). The 151 upregulated genes in apoE4/4 AD had an average FC rank of 12,393.62 (vertical red dotted line), indicating lower ranks and lower expression in response to bumetanide. The 71 downregulated genes in apoE4/4 AD have an average FC rank of 8,815.22 (vertical red line), indicating higher ranks and higher expression in response to bumetanide. Right y-axis denotes number of genes in histogram of scatterplot values. (f, g) Histogram of the FC rank of 1000 permutations of size-matched gene sets taken at random from the bumetanide treatment data from CMap for upregulated genes ($n = 151$) (f) and downregulated genes ($n = 71$) (g) in apoE4/4 AD. The FC rank of human apoE4/4-specific upregulated genes after bumetanide treatment (12,393.62, vertical red dotted line) is significantly higher (Monte Carlo simulation, $P = 0.003$), and that of the downregulated genes after bumetanide (8,815.22, vertical

red line) is significantly lower (Monte Carlo simulation, $P = 0.002$), than the mean of 1000 permutations calculated by Monte Carlo simulation, indicating a shift toward lower expression and higher expression, respectively.

Figure 3

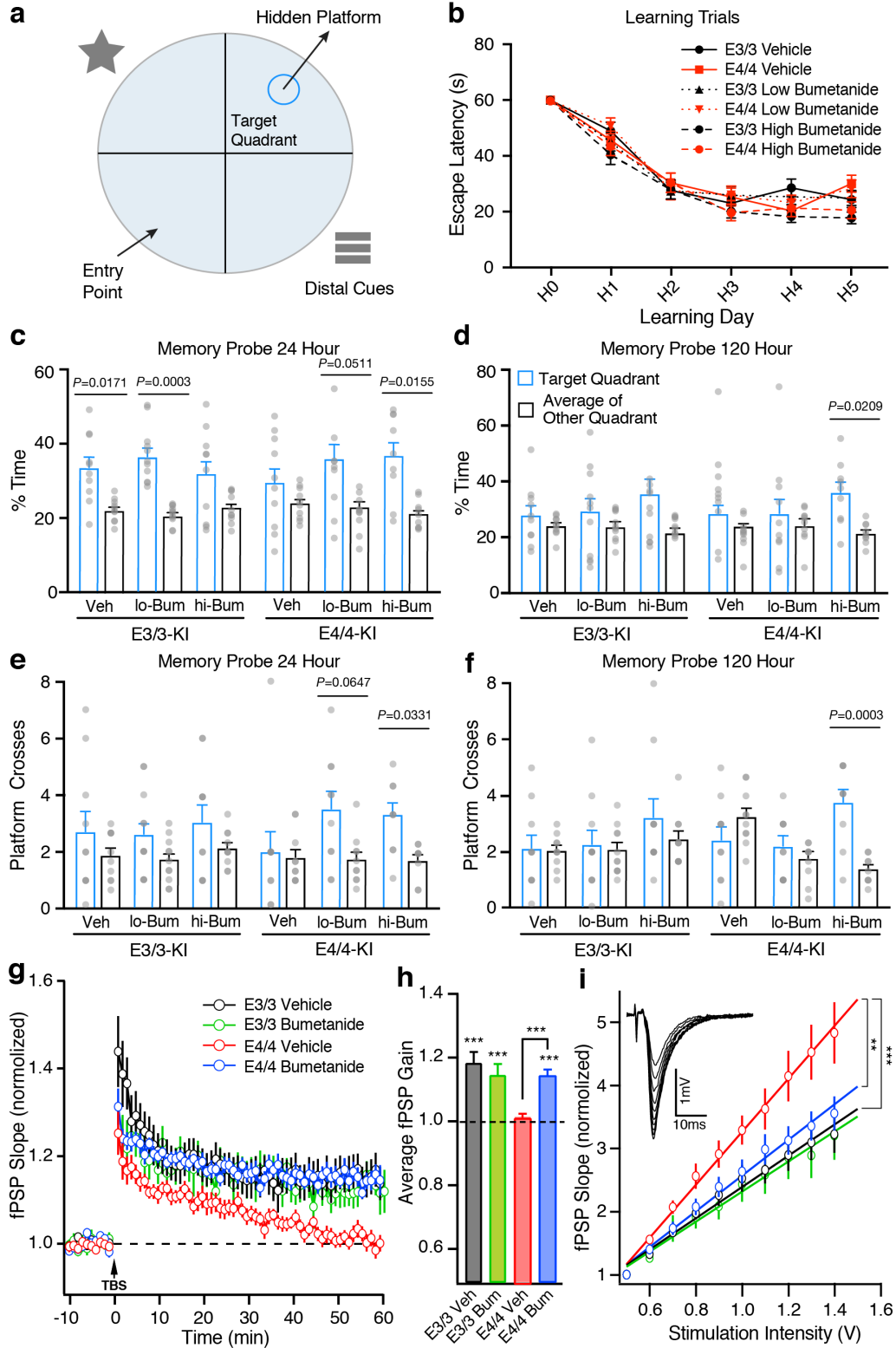


Figure 3. Bumetanide treatment rescues spatial memory deficit specifically in aged apoE4-KI mice. (a) Schematic of the MWM test. Mice are placed in the maze at the entry point and use distal spatial cues to find the hidden platform. (b) Escape latency of bumetanide- (low dose at 0.02 mg/kg and high dose at 0.2 mg/kg daily intraperitoneal injection for 8 weeks) and vehicle-treated apoE3-KI mice (n = 11, 10, and 10, respectively) and apoE4-KI mice (n = 10, 9, and 10 respectively) over learning days 1–5 did not differ between groups. (c) In the 24-hour probe trial, both low and high dose of bumetanide treatment increased percent time apoE4-KI mice spent in the target quadrant versus average percent time in the other quadrants to the level of vehicle-treated apoE3-KI mice. High dose of bumetanide treatment impaired memory of apoE3-KI mice, as compared to vehicle-treated apoE3-KI mice. (d) In the 120-hour probe trial, only high bumetanide-treated apoE4-KI mice spent more time in the target quadrant than controls. (e, f) In 24-hour (e) and 120-hour (f) probe trials, high dose of bumetanide treatment significantly increased platform crossings in target quadrant versus the other quadrants in apoE4-KI mice only. Values are mean \pm SEM. Differences within groups in b–f were determined by paired two-sided *t* test, p-values are as displayed in the figure panels. (g, h) High dose of bumetanide treatment rescued LTP deficit in ex-vivo hippocampal slices from apoE4-KI mice. Theta burst-induced LTP was measured on ex-vivo hippocampal slices from vehicle-treated apoE3-KI mice (n = 14), bumetanide-treated apoE3-KI mice (n = 11), vehicle-treated apoE4-KI mice (n = 14), and bumetanide-treated apoE4-KI mice (n = 12) at ages of 16 months. Average fPSP slope values was binned to one-minute intervals and normalized to control (g). LTP gain outcomes across experimental groups were summarized (h). ApoE vehicle (i) High dose of bumetanide treatment rescued hippocampal network excitability deficit in ex-vivo hippocampal slices from apoE4-KI mice. Input-output relationships in Shaeffer collaterals-CA1 network were measured on ex-vivo hippocampal slices from vehicle-treated apoE3-KI mice (n = 23), bumetanide-treated apoE3-KI mice (n = 10), vehicle-treated apoE4-KI mice (n = 11), and bumetanide-treated apoE4-KI mice (n = 12) at ages of 16 months. The average fPSP slope values (normalized to minimum) across increasing stimulus amplitude were shown. ** p < 0.01; *** p < 0.001.

Figure 4

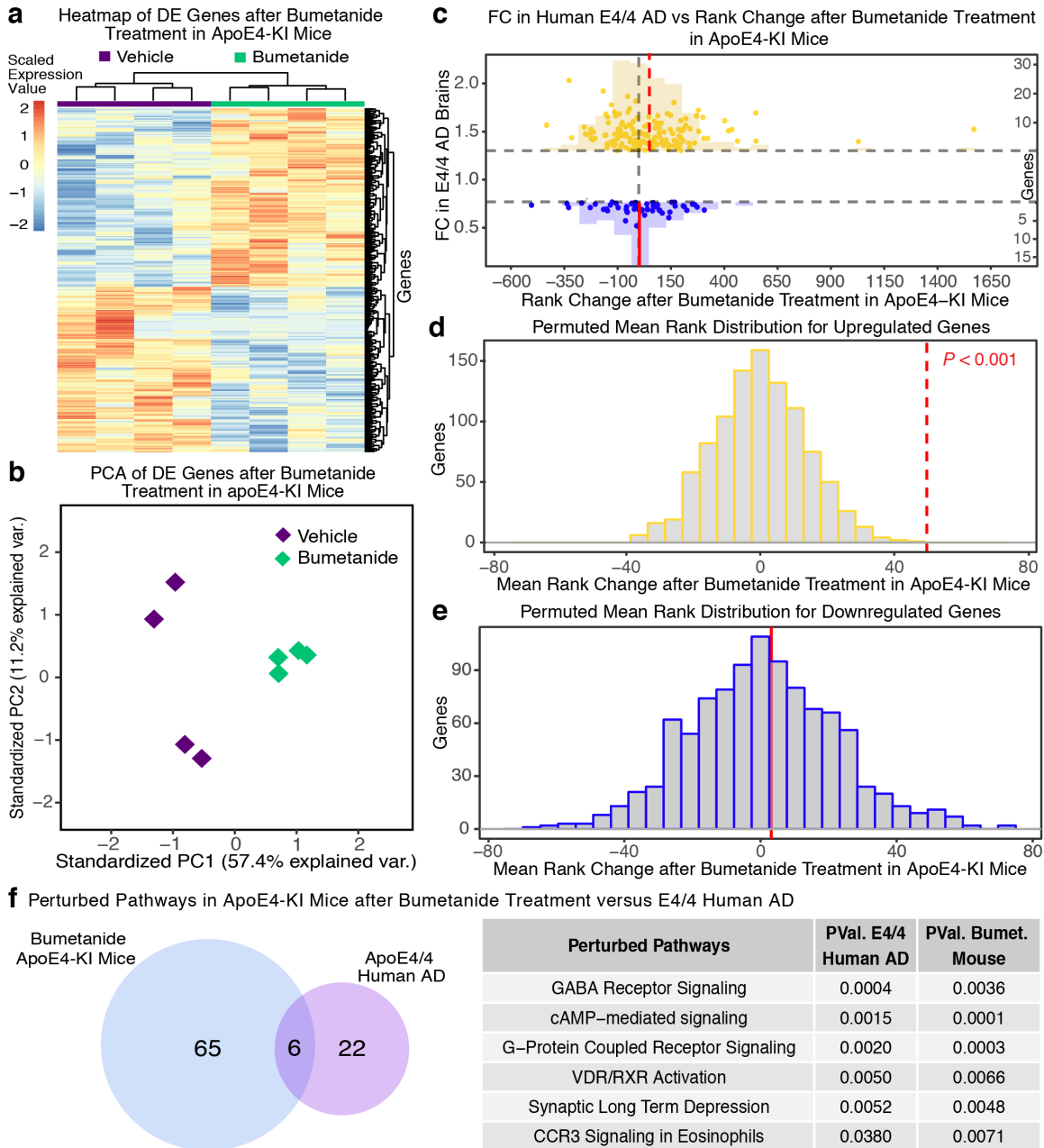


Figure 4. RNA-seq analysis of the transcriptomic perturbation signature of bumetanide in the hippocampus of apoE4-KI mice. (a) Hierarchical clustering analysis of scaled regularized log (rld) transformed RNA expression levels of DE genes ($P < 0.05$) as quantified by RNA-seq of hippocampal tissues from apoE4-KI mice after treatment with bumetanide (0.2 mg/kg intraperitoneal injection for 8 weeks) or vehicle. Color bar denotes scaled rld expression levels. (b) Principal component analysis (PCA) of DE genes in apoE4-KI mouse hippocampal tissues

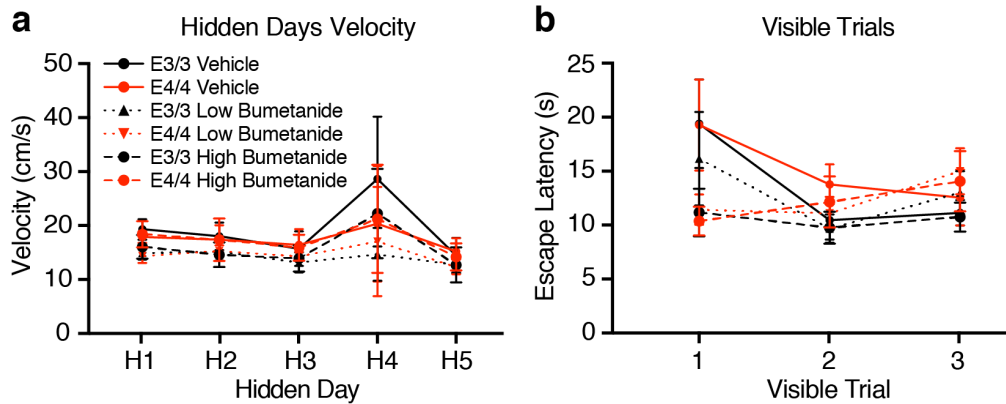
separates bumetanide-treated samples from vehicle-treated samples. Principal component 1 (PC1) accounts for 57.4% and PC2 for 11.2% of the variance. (c) The gene set representing the apoE4/4-specific transcriptomic signature of AD as derived from analysis of human temporal lobe samples (see Figure 1) that were also detected by RNA-seq in apoE4-KI mouse hippocampus. The change in expression rank of these genes in apoE4-KI mouse hippocampal tissues following bumetanide treatment, as compared to vehicle treatment, was plotted against the estimated FC in human temporal lobe samples of apoE4/4 AD as compared to healthy controls. Mean change in expression rank of all genes after bumetanide treatment is zero as expected (vertical gray dotted line). The 157 genes that were upregulated in apoE4/4 human AD had an average change in expression rank of 49.76 (vertical red dotted line) after bumetanide treatment, indicating a shift toward lower ranks and lower expression in response to bumetanide. Right y-axis denotes number of genes in histogram of scatterplot values. (d, e) Histograms of the mean change in expression rank after bumetanide treatment of 1000 random permutations of size-matched gene sets to sets of upregulated genes ($n = 157$) (d) and downregulated genes ($n = 56$) (e) in apoE4/4 AD. The mean change in expression rank of human apoE4/4-specific upregulated genes after bumetanide treatment (49.76, red dotted line) was significantly higher than zero (mean of 1000 permutations) as calculated by Monte Carlo simulation, indicating a significant shift toward lower expression; the mean change in expression rank of downregulated genes was not significantly shifted away from zero. (f) Venn diagram and table of unique (65) and shared (6) significantly enriched ontological pathways by Ingenuity Pathway Analysis (IPA) in DE genes from hippocampus of apoE4-KI mice after bumetanide treatment ($P < 0.05$) as compared to pathways significantly enriched in apoE4/4 AD in humans.

Supplementary Table 1

Supplementary Table 1. Covariate measures for human transcriptomic datasets. For each study separately and combined, the following covariates are reported: apoE status, diagnosis, mean age of each group, SD of within-group age, significance of age difference between controls and AD samples within each genotype (within genotype significance), group size (*n*), number of males, number of females, number of males or females in down-sampled sex-matched groups, within group male to female ratio (Male/Female ratio), and within group male to female ratio after down-sampling (Male/Female ratio down-sample). ApoE3/4 AD samples were significantly older (by 3.24 years) than apoE3/4 control samples in the MayoEGWAS study. This discrepancy was addressed in our computational pipeline as described in Online Methods section.

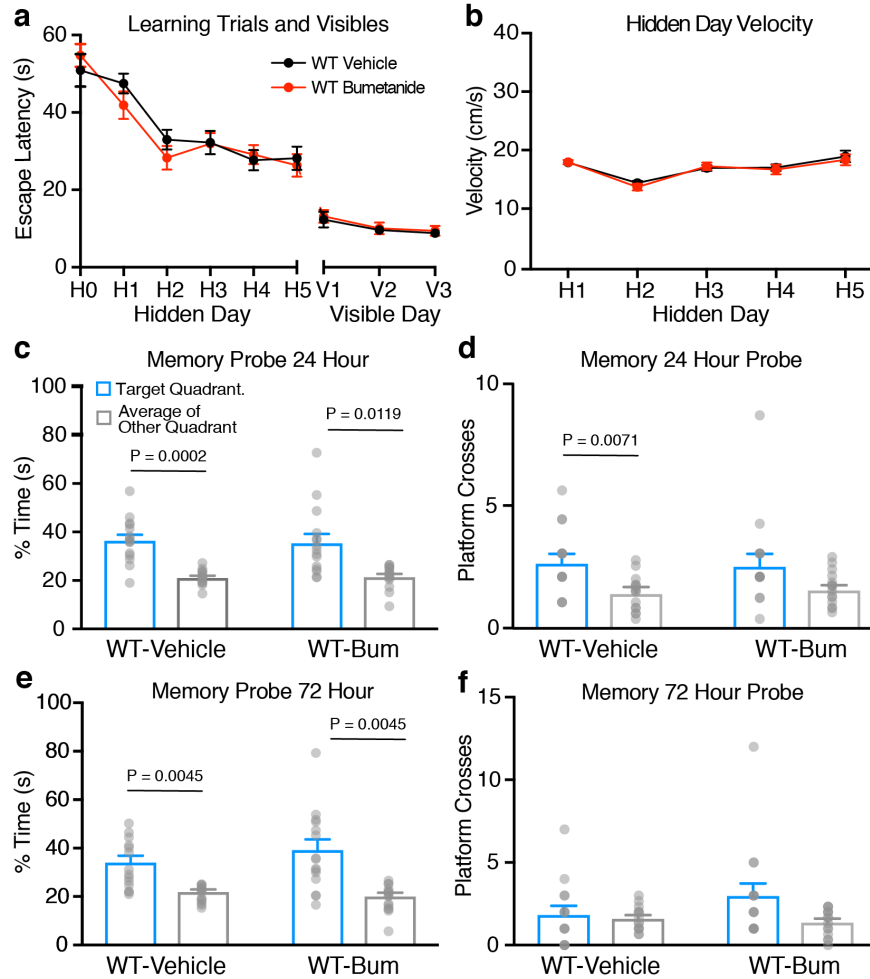
Study	ApoE genotype	Diagnosis	Mean age	SD	Within genotype significance	Total (n)	Male (n)	Male down-sample (n)	Female (n)	Female down-sample (n)	Male/Female ratio	Male/Female ratio down-sample
GSE15222	3/3	Control	81.17	9.20	NS	89	49	32	40	-	1.23	0.80
GSE15222	3/3	AD	84.70	9.10	NS	27	12	-	15	-	0.80	0.80
GSE15222	3/4	Control	79.96	8.18	NS	23	14	-	9	-	1.56	1.56
GSE15222	3/4	AD	83.82	5.21	NS	51	27	-	24	17	1.13	1.59
GSE15222	4/4	Control	71.50	6.76	NS	4	2	-	2	-	1.00	1.00
GSE15222	4/4	AD	81.53	6.10	NS	19	5	-	14	5	0.36	1.00
<u>MayoEGWAS</u>	3/3	Control	71.53	5.43	NS	146	87	40	59	-	1.47	0.68
<u>MayoEGWAS</u>	3/3	AD	73.04	5.86	NS	79	32	-	47	-	0.68	0.68
<u>MayoEGWAS</u>	3/4	Control	71.09	6.09	p = 0.01	46	30	-	16	-	1.88	1.88
<u>MayoEGWAS</u>	3/4	AD	74.32	5.37	p = 0.01	96	50	-	46	27	1.09	1.85
<u>MayoEGWAS</u>	4/4	Control	76.67	2.89	NS	3	2	-	1	-	2.00	2.00
<u>MayoEGWAS</u>	4/4	AD	72.44	4.85	NS	27	12	-	15	6	0.80	2.00
Meta-Analysis	3/3	Control	75.14	8.49	NS	235	136	72	99	-	1.37	0.73
Meta-Analysis	3/3	AD	76.01	8.49	NS	106	44	-	62	-	0.71	0.71
Meta-Analysis	3/4	Control	74.04	8.00	p = 0.02	69	44	-	25	-	1.76	1.76
Meta-Analysis	3/4	AD	77.62	6.97	p = 0.02	147	77	-	70	44	1.10	1.75
Meta-Analysis	4/4	Control	73.71	5.77	NS	7	4	-	3	-	1.33	1.33
Meta-Analysis	4/4	AD	76.20	6.99	NS	46	17	-	29	11	0.59	1.55

Supplementary Figure 1



Supplementary Figure 1. Bumetanide treatment does not affect swim speed or visible trial performance. (a) Bumetanide did not significantly affect swim speed during hidden platform trials of apoE4-KI and apoE3-KI mice. (b) There was no significant difference between any groups in visible trials (measured by 2-way ANOVA), indicating there were no motor or vision impairment in any of the groups.

Supplementary Figure 2

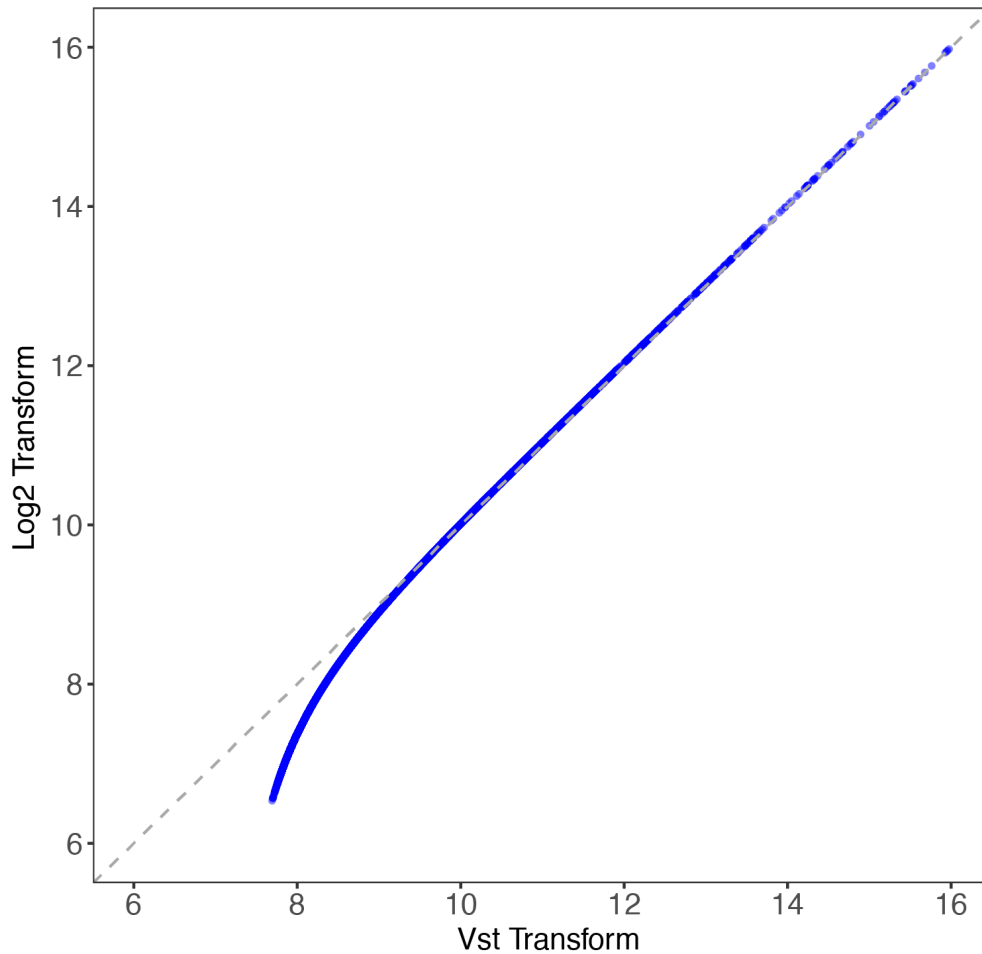


Supplementary Figure 2. The effects of bumetanide treatment in wildtype mice.

(a) Escape latency of vehicle and bumetanide treated WT mice during learning days 1–5 did not differ. (b) Bumetanide did not significantly affect swim speed during hidden platform trials in WT mice as compared to vehicle treated WT controls. (c) In the 24-hour probe trial, both vehicle ($P = 0.0002$) and bumetanide ($P=0.0119$) treated WT mice showed increased percent time spent in the target quadrant versus average percent time in the other quadrants. (d) In the 24-hour probe trials, vehicle treated WT mice showed significantly increased platform crossings ($P=0.0071$) in target quadrant versus the other quadrants, whereas bumetanide treated WT mice did not. (e) In the 72-hour probe trial, both vehicle ($P=0.0045$) and bumetanide ($P=0.0045$) treated WT mice spent more time in the target quadrant than the other quadrants. (f) In the 72-hour probe trial, neither vehicle and bumetanide treated WT animals showed increased target crossings in target quadrant versus the other quadrants. Differences within groups in c–f were determined by paired two-sided t test, p-values are as displayed in the figure panels.

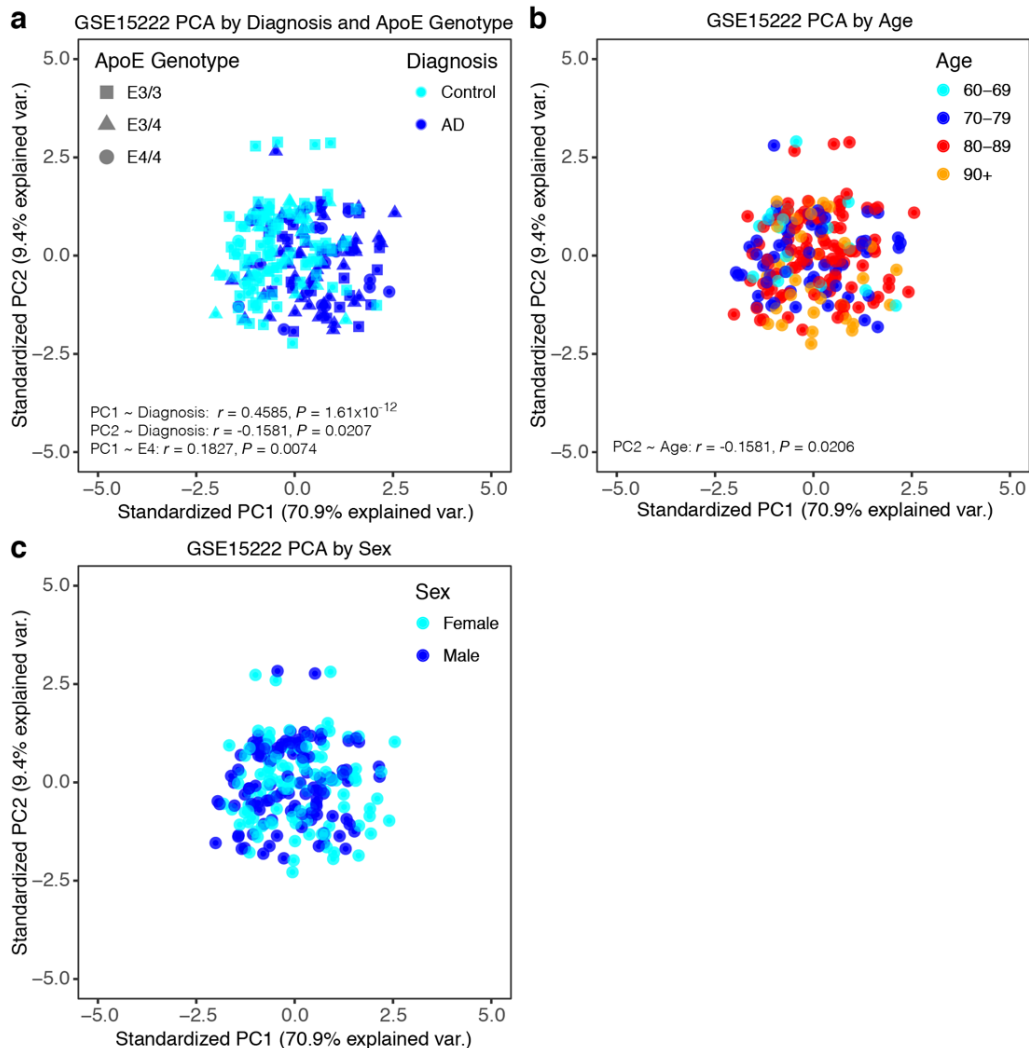
Supplementary Figure 3

Vst Transform vs. Log2 Transform



Supplementary Figure 3. Variance stabilizing transformation deviates from log2 transformation only at lower values. Sample data provided by the lumi package (example.lumi) were downloaded. These data include 8,000 randomly selected genes from Barnes et al., 2005 microarray study¹¹⁸. Vst transformation (lumi package) was plotted against log2 transformation (base R package). Vst values are equal to log2 at higher numbers but begin to deviate upward around a transformed value of 9. Therefore, any fold change calculation from values lower than 9 in a Vst transformation is an underestimation of actual measured fold change.

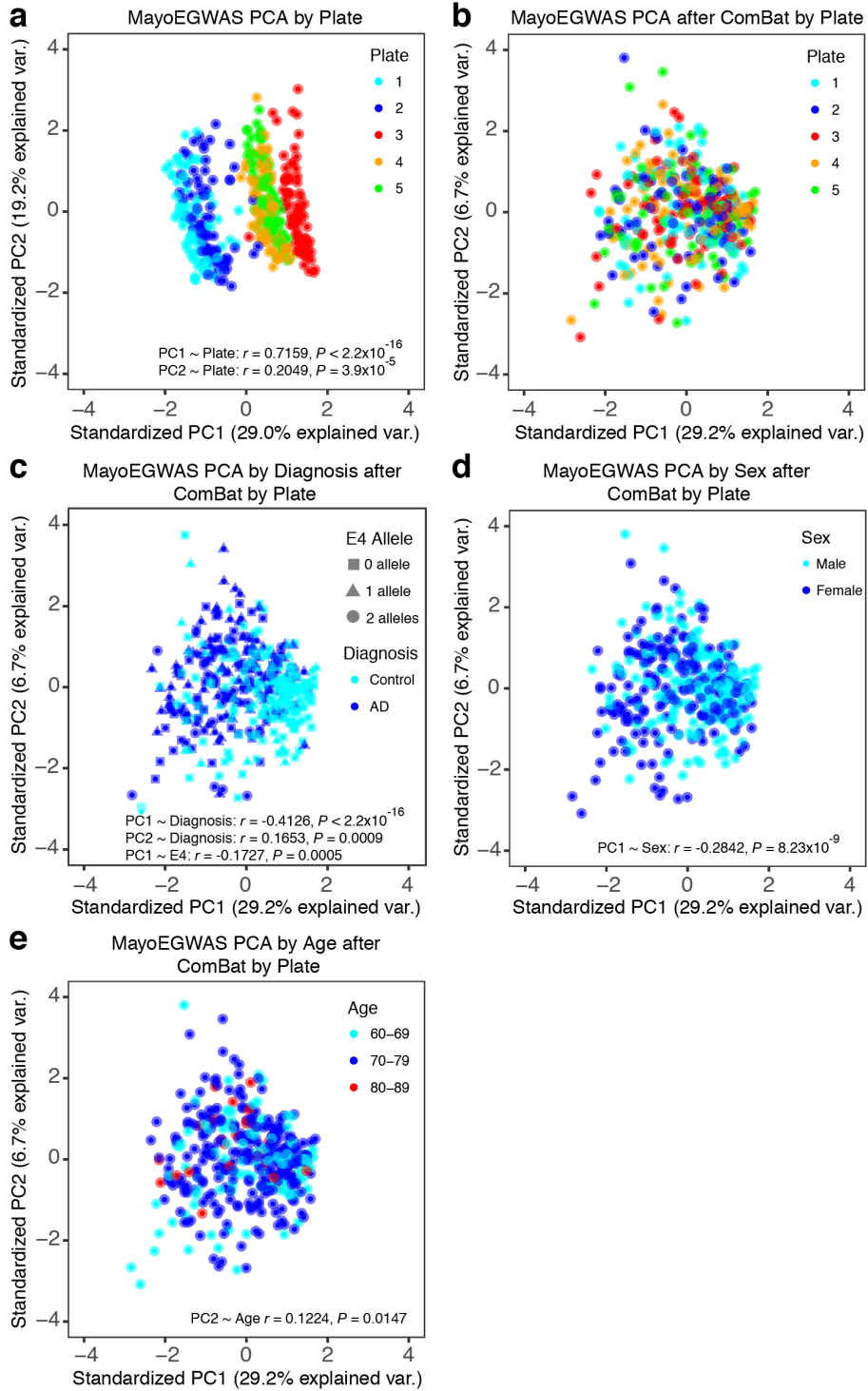
Supplementary Figure 4



Supplementary Figure 4. Principal component analysis of the GSE15222 dataset reveals no clustering trend across apoE4 genotype, diagnosis, age, or sex covariates. (a) GSE15222 was downloaded directly from GEO in the available series matrix file format. Data had been rank invariant normalized as described⁹⁶. The pre-normalization procedure created negative values, which were eliminated by adding a constant across the expression matrix⁹⁹. The data was log2 transformed and the resulting data were subjected to principal component analysis. The first principal component (PC1) was correlated with the diagnosis covariate (Pearson's $r = 0.4585$, $P = 1.61 \times 10^{-12}$). PC2 was also significantly associated with diagnosis (Pearson's $r = -0.1581$, $P = 0.0207$). PC1 was also significantly correlated with apoE4 status (Pearson's $r = 0.1827$, $P = 0.0074$). PC2 did not correlate with diagnosis or apoE4 status. (b) Data displayed according to age decade of sample. PC1 did not correlate with the age covariate. PC2 correlated with age

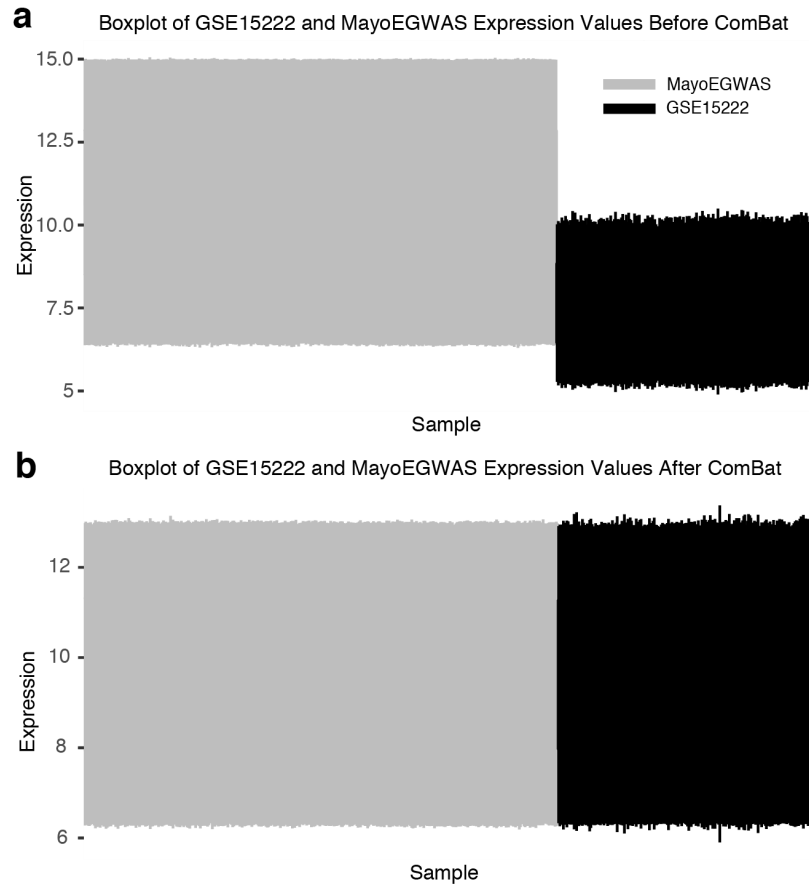
(Pearson's $r = -0.1581$, $P = 0.0206$) (c) Data displayed according to sex. PC1 and PC2 did not correlate with sex.

Supplementary Figure 5



Supplementary Figure 5. Principal component analysis (PCA) of the Syn3157255-MayoEGWAS dataset after batch correction reveals no clustering trend across apoE4 genotype, diagnosis, age, or sex covariates. (a) The Syn3157255-MayoEGWAS dataset was downloaded from the AMP-AD portal. The data had been background corrected and subjected to variance stabilizing transformation (Vst), quantile normalization, and probe filtering with the lumi package of BioConductor, as described¹⁰⁰. Vst transformation is identical to log2 transformation at higher values, but deviates at lower values (see Supplementary Fig. 2)¹⁰¹. The dataset was analyzed by PCA to confirm normalization of technical artifact. A clear technical artifact, corresponding to the “plate” covariate, was apparent across the first principal component (PC1, 29.0% of the explained variance). PC1 correlated with the plate covariate (Pearson $r = 0.7159$, $P < 2.2 \times 10^{-16}$), as did PC2 (Pearson $r = 0.2049$, $P = 3.9 \times 10^{-5}$). (b) The dataset was batch corrected across the plate covariate by using the ComBat function of the sva package, and PCA was done to ensure that the technical artifact had been addressed. PC1 and PC2 did not correlate with the plate covariate after batch correction. (c) The PCA of ComBat-corrected data displayed according to apoE genotype. PC1 correlated with diagnosis (Pearson $r = -0.4126$, $P < 2.2 \times 10^{-16}$), as did PC2 (Pearson $r = 0.1653$, $P = 0.0009$). PC1 correlated with apoE4 allele dosage (Pearson $R^2 = -0.1727$, $P = 0.0005$), but PC2 did not. (d) ComBat-corrected data displayed according to sex. PC1 correlated with sex (Pearson $r = -0.2842$, $P = 8.23 \times 10^{-9}$), but PC2 did not. (e) ComBat-corrected data displayed according to age decade of sample. PC2 correlated with age (Pearson $r = 0.1224$, $P = 0.0147$), and the correlation of PC1 and age approached significance (Pearson $r = -0.0943$, $P = 0.0605$).

Supplementary Figure 6



Supplementary Figure 6. Data integration by probe selection and batch correction yields a normalized dataset for meta-analysis. (a) The Syn3157255-MayoEGWAS dataset was downloaded from the AMP-AD portal. The data had been background corrected and subjected to variance stabilizing transformation (vst), quantile normalization, and probe filtering with the lumi package of BioConductor, as described¹⁰⁰, then batch corrected across the “plate” covariate (see **Supplementary Figure 4**). GSE15222 was downloaded and a constant was applied to the dataset to eliminate negative values; the data were then log₂ transformed. The Limma package was applied to the two datasets separately to estimate differential expression (DE) between all control and AD samples regardless of genotype; for genes with more than one probe, the probe with the most significant *P* value for the difference between AD and control samples was used for subsequent integration¹⁰³. Data were then combined using genes shared in both datasets ($n = 16477$ s). Gene expression values after vst (MayoEGWAS) or log₂ transformation (GSE15222) showed clear differences in expression levels between datasets. (b) Expression values of integrated data after ComBat correction by study show consistency across integrated datasets, which were used for all further DE analysis.

CHAPTER 5: DISCUSSION AND CONCLUSIONS

This study is the first to successfully apply computational drug repositioning to AD in an apoE-genotype-specific manner of precision medicine. We leveraged publically available transcriptomic data to create a precision medicine drug repositioning pipeline for AD which predicted bumetanide as a top candidate against apoE4-mediated AD, with possible efficacy in apoE3/4 and apoE3/3 disease as well. The efficacy of bumetanide for apoE4/4 AD was validated *in vivo* in an apoE4 mouse model of AD via cognitive behavioral testing on the Morris Water Maze. Importantly, the beneficial effects of bumetanide on short- and long-term memories are specific for apoE4 mice at both low and high doses, in some cases allowing these mice to perform at higher levels than both their apoE3 and WT counterparts. Treatment with this drug can actually impair short-term and/or long-term memories in apoE3 and wildtype mice. Further testing bumetanide in clinical trials for apoE4/4 AD is warranted, and since this compound has already received FDA approval, the distance to the clinic is drastically forshortened.

This study validates our strategy to develop new therapies for AD and other neurodegenerative disorders with multifactorial etiology, complicated mechanisms, and patient heterogeneity. Our method addresses the challenges in finding an effective therapy for AD, and highlights the pitfalls of traditional drug discovery pipelines. We successfully circumvented the canonical and perilous one-drug-one-target approach to AD drug development, demonstrating that an unbiased pathway-blind approach to drug discovery may be paramount to success. By allowing the brain to ostensibly speak for itself in the form of large-scale genomic perturbations, we were able to predict efficacious therapies without ascribing to one “causative” pathway or protein. In effect, we hypothesize that drugs capable of perturbing an entire network away from a disease state might be

a more effective treatment strategy for these complex conditions than targeting disease-related individual pathways.

We similarly assert that attempting to develop a single drug suitable for all patients with complex disease may be a severe over-simplification. Combining precision medicine techniques guided by disease-associated gene mutations or polymorphisms with computational drug repositioning is a powerful tool to identify drugs effective for subpopulations of patients, as shown in this study for potential bumetanide treatment of apoE4/4 AD patients only. While AD patients present with similar symptoms and a group of pathological disease markers, it is evident that genetics plays a large role in disease course, and potentially disease causation. We believe strongly that genetic subsets of AD may in fact be separate disorders requiring separate therapeutic approaches, and have approached our drug discovery pipeline with this tenant in mind. We have shown that these genetic factors can be leveraged as powerful tools for targeting personalized drug discovery, and may in fact be inextricably tied to finding successful therapies for AD.

Finally, repurposed drugs that are already FDA approved allow for a faster trajectory to the clinic, which could dramatically lower the cost and shorten the time of drug development pipelines. Mining the repository of >12,000 already FDA-approved compounds is an untapped resource of drugs that need only be re-evaluated for efficacy before reaching the clinic. We believe strongly that by taking advantage of this resource we may be able to hasten drug discovery for diseases that currently have no therapies available.

CHAPTER 6: FUTURE DIRECTIONS

While this study lays the groundwork for precision medicine-assisted computational drug repositioning for Alzheimer's Disease, there are several avenues of research that stem from our initial studies that we believe to be extremely important in our ongoing quest for effective therapies. We hope to build on this first foray into drug repositioning to both create the pipelines and the resources to uncover more and better effective therapies going forward.

Firstly, this study utilizes a pipeline that identifies Bumetanide from the CMap database that was established from tumor cell lines; more precise drug repositioning databases are needed from cell types relevant to neurological diseases, such as neurons and glia. We believe strongly that a cell-type specific repository of FDA approved compounds may be paramount to successful drug discovery, and in this vein are expanding our studies to create such a resource. While the cancer drug line from the CMap served to produce successful results in this baseline study, we are optimistic that more efficacious compounds could be identified with cell-specificity as a factor in our computational screening methods.

Secondly, the human brain studies we relied on for our input to our computational screens rely on a small number of apoE4/4 control individuals. While we were able to produce results with this small n, we are in dire need of more data from non-cognitively impaired apoE4/4 individuals. These persons are exceedingly rare given the large penetrance of the apoE4 allele in homozygotes, however with the advent of personalized genome sequencing technologies, these populations are quickly being identified. Gathering more and better data from these rare populations is extremely important going forward in order to create more accurate screening pipelines for AD therapies.

And lastly, new and better sequencing technologies are continually being developed, and are greatly needed to achieve better granularity in our understanding of the underlying processes

of AD in the human brain. We believe that the timely creation of datasets utilizing single cell sequencing as well as proteomic methods to query the AD brain is of utmost importance to identifying effective therapies against AD, and in a world where 1 in 3 seniors die from this disease, we cannot develop therapies quickly enough.

REFERENCES

1. Huang Y, Mucke L. Alzheimer mechanisms and therapeutic strategies. *Cell*. 2012;148:1204–1222.
2. Golde TE, Schneider LS, Koo EH. Anti-A β therapeutics in Alzheimer's disease: the need for a paradigm shift. *Neuron*. 2011;69:203–213.
3. Corder EH, Saunders AM, Strittmatter WJ, et al. Gene dose of apolipoprotein E type 4 allele and the risk of Alzheimer's disease in late onset families. *Science*. 1993;261:921–923.
4. Huang Y. A β -independent roles of apolipoprotein E4 in the pathogenesis of Alzheimer's disease. *Trends Mol Med* 2010;16:287–294.
5. Mahley RW, Huang Y. Apolipoprotein E sets the stage: response to injury triggers neuropathology. *Neuron*. 2012;76:871–885.
6. Farrer LA, Cupples LA, Haines JL, et al. Effects of age, sex, and ethnicity on the association between apolipoprotein E genotype and Alzheimer disease. A meta-analysis. *J Am Med Assoc*. 1997;278:1349–1356.
7. Genin E, Hannequin D, Wallon D, et al. APOE and Alzheimer disease: a major gene with semi-dominant inheritance. *Mol Psychiatry*. 2011;16:903–907.
8. Lamb J, Crawford ED, Peck D, et al. The Connectivity Map: using gene-expression signatures to connect small molecules, genes, and disease. *Science*. 2006;313:1929–1935.
9. Huang Y. Roles of apolipoprotein E4 (ApoE4) in the pathogenesis of Alzheimer's disease: lessons from ApoE mouse models. *Biochem Soc Trans*. 2011;39(4):924-932.
10. Huang Y, Mucke L. Alzheimer mechanisms and therapeutic strategies. *Cell*. 2012;148(6):1204-1222.

11. Farrer LACLA_vDCMKAZRMUGRCCVSJWD. Apolipoprotein E genotype in patients with Alzheimer's Disease: Implications for the risk of dementia among relatives. *Ann Neurol.* 1995;38(5):797-808.
12. Corder E, Saunders A, Strittmatter W, et al. Gene dose of apolipoprotein E type 4 allele and the risk of Alzheimer's disease in late onset families. *Science.* 1993;261(5123):921-923.
13. Bloom GS. Amyloid-beta and tau: the trigger and bullet in Alzheimer disease pathogenesis. *JAMA Neurol.* 2014;71(4):505-508.
14. Golde TE, Schneider LS, Koo EH. Anti- β therapeutics in Alzheimer's disease: the need for a paradigm shift. *Neuron.* 2011;69(2):203-213.
15. Mangialasche F, Solomon A, Winblad B, Mecocci P, Kivipelto M. Alzheimer's disease: clinical trials and drug development. *The Lancet Neurology.* 2010;9(7):702-716.
16. Krstic D, Knuesel I. Deciphering the mechanism underlying late-onset Alzheimer disease. *Nature reviews Neurology.* 2013;9(1):25-34.
17. Corder EH, Ghebremedhin E, Taylor MG, Thal DR, Ohm TG, Braak H. The biphasic relationship between regional brain senile plaque and neurofibrillary tangle distributions: modification by age, sex, and APOE polymorphism. *Annals of the New York Academy of Sciences.* 2004;1019:24-28.
18. Reiman EM, Chen K, Alexander GE, et al. Functional brain abnormalities in young adults at genetic risk for late-onset Alzheimer's dementia. *Proceedings of the National Academy of Sciences of the United States of America.* 2004;101(1):284-289.
19. Jagust WJ, Landau SM. Apolipoprotein E, not fibrillar beta-amyloid, reduces cerebral glucose metabolism in normal aging. *J Neurosci.* 2012;32(50):18227-18233.

20. Brecht WJ, Harris FM, Chang S, et al. Neuron-specific apolipoprotein ϵ 4 proteolysis is associated with increased tau phosphorylation in brains of transgenic mice. *J Neurosci*. 2004;24(10):2527-2534.
21. Jofre-Monseny L, Minihane AM, Rimbach G. Impact of apoE genotype on oxidative stress, inflammation and disease risk. *Molecular nutrition & food research*. 2008;52(1):131-145.
22. Andrews-Zwilling Y, Bien-Ly N, Xu Q, et al. Apolipoprotein E4 causes age- and Tau-dependent impairment of GABAergic interneurons, leading to learning and memory deficits in mice. *J Neurosci*. 2010;30(41):13707-13717.
23. Knoferle J, Yoon SY, Walker D, et al. Apolipoprotein E4 produced in GABAergic interneurons causes learning and memory deficits in mice. *J Neurosci*. 2014;34:14069–14078.
24. Leung L, Andrews-Zwilling Y, Yoon SY, et al. Apolipoprotein E4 causes age- and sex-dependent impairments of hilar GABAergic interneurons and learning and memory deficits in mice. *PLoS One*. 2012;7(12):e53569.
25. Brodbeck J, Balestra ME, Saunders AM, Roses AD, Mahley RW, Huang Y. Rosiglitazone increases dendritic spine density and rescues spine loss caused by apolipoprotein E4 in primary cortical neurons. *Proceedings of the National Academy of Sciences of the United States of America*. 2008;105(4):1343-1346.
26. Hung SY, Fu WM. Drug candidates in clinical trials for Alzheimer's disease. *Journal of biomedical science*. 2017;24(1):47.
27. Corbett A, Smith J, Ballard C. New and emerging treatments for Alzheimer's disease. *Expert review of neurotherapeutics*. 2012;12(5):535-543.

28. Nygaard HB. Current and emerging therapies for Alzheimer's disease. *Clinical therapeutics*. 2013;35(10):1480-1489.
29. Wang CH, Wang LS, Zhu N. Cholinesterase inhibitors and non-steroidal anti-inflammatory drugs as Alzheimer's disease therapies: an updated umbrella review of systematic reviews and meta-analyses. *European review for medical and pharmacological sciences*. 2016;20(22):4801-4817.
30. Zhong N, Weisgraber KH. Understanding the association of apolipoprotein E4 with Alzheimer disease: clues from its structure. *The Journal of biological chemistry*. 2009;284(10):6027-6031.
31. Zhang M, Schmitt-Ulms G, Sato C, et al. Drug Repositioning for Alzheimer's Disease Based on Systematic 'omics' Data Mining. *PLoS One*. 2016;11(12):e0168812.
32. Zhang SD, Gant TW. A simple and robust method for connecting small-molecule drugs using gene-expression signatures. *BMC Bioinformatics*. 2008;9:258.
33. Parsons CG. CNS repurposing - Potential new uses for old drugs: Examples of screens for Alzheimer's disease, Parkinson's disease and spasticity. *Neuropharmacology*. 2019;147:4-10.
34. Reitz C. Toward precision medicine in Alzheimer's disease. *Annals of translational medicine*. 2016;4(6):107.
35. Yu L, Chibnik LB, Srivastava GP, et al. Association of Brain DNA methylation in SORL1, ABCA7, HLA-DRB5, SLC24A4, and BIN1 with pathological diagnosis of Alzheimer disease. *JAMA Neurol*. 2015;72(1):15-24.

36. Bigler ED, Kerr B, Victoroff J, Tate DF, Breitner JC. White matter lesions, quantitative magnetic resonance imaging, and dementia. *Alzheimer disease and associated disorders*. 2002;16(3):161-170.
37. Chakrabarty P, Li A, Ceballos-Diaz C, et al. IL-10 alters immunoproteostasis in APP mice, increasing plaque burden and worsening cognitive behavior. *Neuron*. 2015;85(3):519-533.
38. Ameen-Ali KE, Wharton SB, Simpson JE, Heath PR, Sharp P, Berwick J. Review: Neuropathology and behavioural features of transgenic murine models of Alzheimer's disease. *Neuropathology and applied neurobiology*. 2017;43(7):553-570.
39. Lotfi Shahreza M, Ghadiri N, Mousavi SR, Varshosaz J, Green JR. A review of network-based approaches to drug repositioning. *Brief Bioinform*. 2018;19(5):878-892.
40. Siavelis JC, Bourdakou MM, Athanasiadis EI, Spyrou GM, Nikita KS. Bioinformatics methods in drug repurposing for Alzheimer's disease. *Brief Bioinform*. 2016;17(2):322-335.
41. Dudley JT, Sirota M, Shenoy M, et al. Computational repositioning of the anticonvulsant topiramate for inflammatory bowel disease. *Sci Transl Med*. 2011;3:96ra76.
42. Sirota M, Dudley JT, Kim J, et al. Discovery and preclinical validation of drug indications using compendia of public gene expression data. *Sci Transl Med*. 2011;3:96ra77.
43. Cheng F, Liu C, Jiang J, et al. Prediction of drug-target interactions and drug repositioning via network-based inference. *PLoS Comput Biol*. 2012;8:e1002503.
44. Chen B, Wei W, Ma L, et al. Computational Discovery of Niclosamide Ethanolamine, a Repurposed Drug Candidate That Reduces Growth of Hepatocellular Carcinoma Cells In

- Vitro and in Mice by Inhibiting Cell Division Cycle 37 Signaling. *Gastroenterology*. 2017;152:2022–2036.
45. Katare PB, Banerjee SK. Repositioning of Drugs in Cardiometabolic Disorders: Importance and Current Scenario. *Current topics in medicinal chemistry*. 2016;16(19):2189-2200.
46. Minaz N, Razdan R, Pathak L. Repositioning of molsidomine for its efficacy in diabetes induced erectile dysfunction in rats: In silico, in vitro and in vivo approach. *Pharmacological reports : PR*. 2018;70(2):309-315.
47. Morales-Rosado JA, Cousin MA, Ebbert JO, Klee EW. A Critical Review of Repurposing Apomorphine for Smoking Cessation. *Assay and drug development technologies*. 2015;13(10):612-622.
48. Faraone SV, Zhang-James Y. Can sodium/hydrogen exchange inhibitors be repositioned for treating attention deficit hyperactivity disorder? An in silico approach. *American journal of medical genetics Part B, Neuropsychiatric genetics : the official publication of the International Society of Psychiatric Genetics*. 2013;162b(7):711-717.
49. Napolitano F, Zhao Y, Moreira VM, et al. Drug repositioning: a machine-learning approach through data integration. *Journal of cheminformatics*. 2013;5(1):30.
50. Morgan S, Grootendorst P, Lexchin J, Cunningham C, Greyson D. The cost of drug development: a systematic review. *Health policy (Amsterdam, Netherlands)*. 2011;100(1):4-17.
51. Singhal S, Mehta J. Thalidomide in cancer: potential uses and limitations. *BioDrugs : clinical immunotherapeutics, biopharmaceuticals and gene therapy*. 2001;15(3):163-172.

52. Wishart DS, Feunang YD, Guo AC, et al. DrugBank 5.0: a major update to the DrugBank database for 2018. *Nucleic acids research*. 2018;46(D1):D1074-d1082.
53. Seiler KP, George GA, Happ MP, et al. ChemBank: a small-molecule screening and cheminformatics resource database. *Nucleic acids research*. 2008;36(Database issue):D351-359.
54. Chen X, Ji ZL, Chen YZ. TTD: Therapeutic Target Database. *Nucleic acids research*. 2002;30(1):412-415.
55. Barbarino JM, Whirl-Carrillo M, Altman RB, Klein TE. PharmGKB: A worldwide resource for pharmacogenomic information. *Wiley interdisciplinary reviews Systems biology and medicine*. 2018;10(4):e1417.
56. Ahmed J, Meinel T, Dunkel M, et al. CancerResource: a comprehensive database of cancer-relevant proteins and compound interactions supported by experimental knowledge. *Nucleic acids research*. 2011;39(Database issue):D960-967.
57. Wu C, Gudivada RC, Aronow BJ, Jegga AG. Computational drug repositioning through heterogeneous network clustering. *BMC systems biology*. 2013;7 Suppl 5:S6.
58. Wu H, Gao L, Dong J, Yang X. Detecting overlapping protein complexes by rough-fuzzy clustering in protein-protein interaction networks. *PLoS One*. 2014;9(3):e91856.
59. Shannon P, Markiel A, Ozier O, et al. Cytoscape: a software environment for integrated models of biomolecular interaction networks. *Genome research*. 2003;13(11):2498-2504.
60. Keenan AB, Jenkins SL, Jagodnik KM, et al. The Library of Integrated Network-Based Cellular Signatures NIH Program: System-Level Cataloging of Human Cells Response to Perturbations. *Cell systems*. 2018;6(1):13-24.

61. Kim J, Yoo M, Kang J, Tan AC. K-Map: connecting kinases with therapeutics for drug repurposing and development. *Human genomics*. 2013;7:20.
62. Alaimo S, Bonnici V, Cancemi D, Ferro A, Giugno R, Pulvirenti A. DT-Web: a web-based application for drug-target interaction and drug combination prediction through domain-tuned network-based inference. *BMC systems biology*. 2015;9 Suppl 3:S4.
63. Ma X, Xu L, Alberobello AT, et al. Celastrol Protects against Obesity and Metabolic Dysfunction through Activation of a HSF1-PGC1alpha Transcriptional Axis. *Cell metabolism*. 2015;22(4):695-708.
64. Sun Y, Sheng Z, Ma C, et al. Combining genomic and network characteristics for extended capability in predicting synergistic drugs for cancer. *Nature communications*. 2015;6:8481.
65. Qu XA, Rajpal DK. Applications of Connectivity Map in drug discovery and development. *Drug discovery today*. 2012;17(23-24):1289-1298.
66. Chen X, Zang W, Xue F, Shen Z, Zhang Q. Bioinformatics analysis reveals potential candidate drugs for different subtypes of glioma. *Neurological sciences : official journal of the Italian Neurological Society and of the Italian Society of Clinical Neurophysiology*. 2013;34(7):1139-1143.
67. Yuen T, Iqbal J, Zhu LL, et al. Disease-drug pairs revealed by computational genomic connectivity mapping on GBA1 deficient, Gaucher disease mice. *Biochemical and biophysical research communications*. 2012;422(4):573-577.
68. Raghavan R, Hyter S, Pathak HB, et al. Drug discovery using clinical outcome-based Connectivity Mapping: application to ovarian cancer. *BMC genomics*. 2016;17(1):811.

69. Musa A, Ghoraie LS, Zhang SD, et al. A review of connectivity map and computational approaches in pharmacogenomics. *Brief Bioinform.* 2018;19(3):506-523.
70. Isozaki Y, Hoshino I, Akutsu Y, et al. Screening of alternative drugs to the tumor suppressor miR-375 in esophageal squamous cell carcinoma using the connectivity map. *Oncology.* 2014;87(6):351-363.
71. Xiong DD, Dang YW, Lin P, et al. A circRNA-miRNA-mRNA network identification for exploring underlying pathogenesis and therapy strategy of hepatocellular carcinoma. *Journal of translational medicine.* 2018;16(1):220.
72. Webster JA, Gibbs JR, Clarke J, et al. Genetic control of human brain transcript expression in Alzheimer disease. *Am J Hum Genet.* 2009;84(4):445-458.
73. Li J, Zhu X, Chen JY. Building disease-specific drug-protein connectivity maps from molecular interaction networks and PubMed abstracts. *PLoS Comput Biol.* 2009;5(7):e1000450.
74. Liu W, Tu W, Li L, et al. Revisiting Connectivity Map from a gene co-expression network analysis. *Experimental and therapeutic medicine.* 2018;16(2):493-500.
75. Puskarjov M, Kahle KT, Ruusuvoori E, Kaila K. Pharmacotherapeutic targeting of cation-chloride cotransporters in neonatal seizures. *Epilepsia.* 2014;55(6):806-818.
76. Brater DC. Benefits and risks of torasemide in congestive heart failure and essential hypertension. *Drug safety.* 1996;14(2):104-120.
77. Brater DC. Clinical pharmacology of loop diuretics in health and disease. *European heart journal.* 1992;13 Suppl G:10-14.
78. Brater DC. Disposition and response to bumetanide and furosemide. *The American journal of cardiology.* 1986;57(2):20a-25a.

79. Brater DC, Day B, Burdette A, Anderson S. Bumetanide and furosemide in heart failure. *Kidney international*. 1984;26(2):183-189.
80. Hasannejad H, Takeda M, Taki K, et al. Interactions of human organic anion transporters with diuretics. *The Journal of pharmacology and experimental therapeutics*. 2004;308(3):1021-1029.
81. Bourke E, Asbury MJ, O'Sullivan S, Gatenby PB. The sites of action of bumetanide in man. *European journal of pharmacology*. 1973;23(3):283-289.
82. Imai M. Effect of bumetanide and furosemide on the thick ascending limb of Henle's loop of rabbits and rats perfused in vitro. *European journal of pharmacology*. 1977;41(4):409-416.
83. McGahan MC, Yorio T, Bentley PJ. The mode of action of bumetanide: inhibition of chloride transport across the amphibian cornea. *The Journal of pharmacology and experimental therapeutics*. 1977;203(1):97-102.
84. Haas M, McManus TJ. Bumetanide inhibits (Na + K + 2Cl) co-transport at a chloride site. *The American journal of physiology*. 1983;245(3):C235-240.
85. Dzhala VI, Talos DM, Sdrulla DA, et al. NKCC1 transporter facilitates seizures in the developing brain. *Nature medicine*. 2005;11(11):1205-1213.
86. Nardou R, Ben-Ari Y, Khalilov I. Bumetanide, an NKCC1 antagonist, does not prevent formation of epileptogenic focus but blocks epileptic focus seizures in immature rat hippocampus. *Journal of neurophysiology*. 2009;101(6):2878-2888.
87. Deidda G, Parrini M, Naskar S, Bozarth IF, Contestabile A, Cancedda L. Reversing excitatory GABAAR signaling restores synaptic plasticity and memory in a mouse model of Down syndrome. *Nature medicine*. 2015;21(4):318-326.

88. Brandt C, Nozadze M, Heuchert N, Rattka M, Loscher W. Disease-modifying effects of phenobarbital and the NKCC1 inhibitor bumetanide in the pilocarpine model of temporal lobe epilepsy. *J Neurosci*. 2010;30(25):8602-8612.
89. Hadjikhani N, Zurcher NR, Rogier O, et al. Improving emotional face perception in autism with diuretic bumetanide: a proof-of-concept behavioral and functional brain imaging pilot study. *Autism : the international journal of research and practice*. 2015;19(2):149-157.
90. Lemonnier E, Degrez C, Phelep M, et al. A randomised controlled trial of bumetanide in the treatment of autism in children. *Translational psychiatry*. 2012;2:e202.
91. Suvitayavat W, Palfrey HC, Haas M, Dunham PB, Kalmar F, Rao MC. Characterization of the endogenous Na(+)-K(+)-2Cl⁻ cotransporter in *Xenopus* oocytes. *The American journal of physiology*. 1994;266(1 Pt 1):C284-292.
92. Beck J, Lenart B, Kintner DB, Sun D. Na-K-Cl cotransporter contributes to glutamate-mediated excitotoxicity. *J Neurosci*. 2003;23(12):5061-5068.
93. Pentikainen PJ, Penttila A, Neuvonen PJ, Gothoni G. Fate of [¹⁴C]-bumetanide in man. *British journal of clinical pharmacology*. 1977;4(1):39-44.
94. Lee SH, Lee MG, Kim ND. Pharmacokinetics and pharmacodynamics of bumetanide after intravenous and oral administration to rats: absorption from various GI segments. *Journal of pharmacokinetics and biopharmaceutics*. 1994;22(1):1-17.
95. Sivakumaran S, Maguire J. Bumetanide reduces seizure progression and the development of pharmacoresistant status epilepticus. *Epilepsia*. 2016;57(2):222-232.
96. Webster JA, Gibbs JR, Clarke J, et al. Genetic control of human brain transcript expression in Alzheimer disease. *Am J Hum Genet*. 2009;84:445-458.

97. Edgar R, Domrachev M, Lash AE. Gene Expression Omnibus: NCBI gene expression and hybridization array data repository. *Nucleic Acids Res.* 2002;30:207–210.
98. Workman C, Jensen LJ, Jarmer H, et al. A new non-linear normalization method for reducing variability in DNA microarray experiments. *Genome Biol.* 2002;3:research0048.0041–0048.0016.
99. Sharov AA, Schlessinger D, Ko MS. ExAtlas: An interactive online tool for meta-analysis of gene expression data. *J Bioinform Comput Biol.* 2015;13:1550019.
100. Zou F, Chai HS, Younkin CS, et al. Brain expression genome-wide association study (eGWAS) identifies human disease-associated variants. *PLoS Genet.* 2012;8:e1002707.
101. Durbin BP, Hardin JS, Hawkins DM, Rocke DM. A variance-stabilizing transformation for gene-expression microarray data. *Bioinformatics.* 2002;18:S105–S110.
102. Leek JT, Johnson WE, Parker HS, Jaffe AE, Storey JD. The sva package for removing batch effects and other unwanted variation in high-throughput experiments. *Bioinformatics.* 2012;28:882–883.
103. Siavelis JC, Bourdakou MM, Athanasiadis EI, Spyrou GM, Nikita KS. Bioinformatics methods in drug repurposing for Alzheimer's disease. *Brief Bioinform.* 2016;17:322–335.
104. Hong F, Breitling R, McEntee CW, Wittner BS, Nemhauser JL, Chory J. RankProd: a bioconductor package for detecting differentially expressed genes in meta-analysis. *Bioinformatics.* 2006;22:2825–2827.
105. Hamanaka H, Kato-Fukui Y, Suzuki K, et al. Altered cholesterol metabolism in human apolipoprotein E4 knock-in mice. *Hum Mol Genet.* 2000;9:353–361.

106. Sullivan PM, Mace BE, Maeda N, Schmechel DE. Marked regional differences of brain human apolipoprotein E expression in targeted replacement mice. *Neuroscience*. 2004;124:725–733.
107. Andrews-Zwilling Y, Bien-Ly N, Xu Q, et al. Apolipoprotein E4 causes age- and Tau-dependent impairment of GABAergic interneurons, leading to learning and memory deficits in mice. *J Neurosci*. 2010;30:13707–13717.
108. Leung L, Andrews-Zwilling Y, Yoon SY, et al. Apolipoprotein E4 causes age- and sex-dependent impairments of hilar GABAergic interneurons and learning and memory deficits in mice. *PLoS ONE*. 2012;7:e53569.
109. Tong LM, Djukic B, Arnold C, et al. Inhibitory interneuron progenitor transplantation restores normal learning and memory in apoE4 knock-in mice without or with A β accumulation. *J Neurosci*. 2014;34:9506–9515.
110. Raber J, Wong D, Buttini M, et al. Isoform-specific effects of human apolipoprotein E on brain function revealed in *ApoE* knockout mice: Increased susceptibility of females. *Proc Natl Acad Sci USA*. 1998;95:10914–10919.
111. Dobin A, Davis CA, Schlesinger F, et al. STAR: ultrafast universal RNA-seq aligner. *Bioinformatics*. 2013;29:15–21.
112. Liao Y, Smyth GK, Shi W. featureCounts: an efficient general purpose program for assigning sequence reads to genomic features. *Bioinformatics*. 2014;30:923–930.
113. Robinson MD, McCarthy DJ, Smyth GK. edgeR: a Bioconductor package for differential expression analysis of digital gene expression data. *Bioinformatics*. 2010;26:139–140.

114. Csermely P, Korcsmaros T, Kiss HJ, London G, Nussinov R. Structure and dynamics of molecular network: a novel paradigm of drug discovery: a comprehensive review. *Pharmacol Ther.* 2013;138:333–408.
115. Chen B, Ma L, Paik H, et al. Reversal of cancer gene expression correlates with drug efficacy and reveals therapeutic targets. *Nat Commun.* 2017;8:16022.
116. Chen B, Butte AJ. Leveraging big data to transform target selection and drug discovery. *Clin Pharmacol Ther.* 2016;99:285–297.
117. Cai X, Chen Y, Gao Z, Xu R. Explore Small Molecule-induced Genome-wide Transcriptional Profiles for Novel Inflammatory Bowel Disease Drug. *AMIA Jt Summits Transl Sci Proc.* 2016;2016:22–31.
118. Barnes M, Freudenberg J, Thompson S, Aronow B, Pavlidis P. Experimental comparison and cross-validation of the Affymetrix and Illumina gene expression analysis platforms. *Nucleic Acids Res.* 2005;33:5914–5923.

Publishing Agreement

It is the policy of the University to encourage the distribution of all theses, dissertations, and manuscripts. Copies of all UCSF theses, dissertations, and manuscripts will be routed to the library via the Graduate Division. The library will make all theses, dissertations, and manuscripts accessible to the public and will preserve these to the best of their abilities, in perpetuity.

Please sign the following statement:

I hereby grant permission to the Graduate Division of the University of California, San Francisco to release copies of my thesis, dissertation, or manuscript to the Campus Library to provide access and preservation, in whole or in part, in perpetuity.

Ali Tavhes

Author Signature

3.28.19

Date